Intracellular Factor H drives tumor progression independently of the complement cascade

Marie V Daugan, Margot Revel, Romane Thouenon, Marie-Agnes Dragon-Durey, Tania Robe-Rybkine, Carine Torset, Nicolas S Merle, Remi Noe, Virginie Verkarre, Stephane M Oudard, et al.

Intracellular Factor H drives tumor progression independently of the complement cascade

Marie V. Daugan[1#], Margot Revel[1#], Romane Thouenon[1], Marie-Agnès Dragon-Durey[1,2], Tania Robe-Rybkine[1], Carine Torset[1], Nicolas S. Merle[1], Rémi Noé[1], Virginie Verkarre[3,4], Stephane Marie Oudard[3,5], Arnaud Mejean[3,6], Pierre Validire[7], Xavier Cathelineau[3,8], Rafael Sanchez-Salas[8], Mathew C. Pickering[9], Isabelle Cremer[1], Audrey Mansuet-Lupo[1,10], Marco Alifano[1,10], Catherine Sautés-Fridman[1], Diane Damotte[1,10], Wolf H. Fridman[1], Lubka T. Roumenina[1*]

1 Centre de Recherche des Cordeliers, INSERM, Sorbonne Université, Université de Paris, Team Inflammation, complement and cancer, F-75006 Paris, France.

2 Hôpital Européen Georges-Pompidou, Biologic Immunology Department, Assistance Publique Hopitaux de Paris, F-75015, France.

3 Université de Paris, F-75006, Paris, France.

4 Hôpital Européen Georges-Pompidou, Pathology Department, Assistance Publique Hopitaux de Paris, F-75015, France.

5 Hôpital Européen Georges-Pompidou, Oncology Department, Assistance Publique Hopitaux de Paris, France.

6 Hôpital Européen Georges-Pompidou, Urology Department, Assistance Publique Hopitaux de Paris, F-75015, France.

7 Institut Mutualiste Montsouris, Department of Pathology, Paris, France.

8 Institut Mutualiste Montsouris, Department of Urology, Paris, France.

9 Centre for Complement and Inflammation Research, Imperial College, London, United Kingdom.

10 Hôpital Cochin, Departments of Pathology and Thoracic Surgery, Assistance Publique Hopitaux de Paris, F-75014 France.

[#]**Equal contribution**

[*]**Correspondence to**: Lubka T. Roumenina, Ph.D., Cordeliers Research Center, INSERM UMRS 1138, 15 rue de l'Ecole de Medecine, 75006 Paris, France; Phone: 33-1-44-27-90-96/Fax: 33-1-40-51-04-20 ; E-mail: lubka.roumenina@sorbonne-universite.fr

Running title: Intracellular Factor H drives cancer progression

Keywords: complement system, complement factor H, intracellular complement, clear cell renal cell carcinoma, lung adenocarcinoma

Funding information: This work was supported by grants from the Cancer Research for Personalized Medicine (CARPEM) and ARC contre le cancer and La Ligue contre le cancer to LTR and équipe

labellisée Ligue contre le cancer (WHF and CSF). This work was also supported by INSERM, University of Paris, Sorbonne University, and the Labex Immuno-Oncology Excellence Program. MVD received a Ph.D. fellowship from ARC.

Authors' disclosures: The authors declare no conflicts of interest

Synopsis: The complement regulator Factor H (FH) is shown to exert protumoral actions through an intracellular, noncanonical mechanism that alters proliferation, cell cycle, morphology, and migration in clear cell renal cell carcinoma and lung adenocarcinoma.

Abstract

The complement system is a powerful and druggable innate immune component of the tumor microenvironment. Nevertheless, it is challenging to elucidate the exact mechanisms by which complement affects tumor growth. In this study, we examined the processes by which the master complement regulator Factor H (FH) affects clear cell renal cell carcinoma (ccRCC) and lung cancer, two cancers in which complement overactivation predicts poor prognosis. FH was present in two distinct cellular compartments: the membranous (mb-FH) and intracellular (int-FH) compartments. Int-FH resided in lysosomes and colocalized with C3. In ccRCC and lung adenocarcinoma FH exerted protumoral action through an intracellular, noncanonical mechanism. FH silencing in ccRCC cell lines resulted in decreased proliferation, due to cell cycle arrest and increased mortality, and this was associated with increased p53 phosphorylation and NF-κB translocation to the nucleus. Moreover, the migration of the FH-silenced cells was reduced, likely due to altered morphology. These effects were cell type–specific since no modifications occurred upon *CFH* silencing in other FH-expressing cells tested: tubular cells (from which ccRCC originates), endothelial cells (HUVECs) and squamous cell lung cancer cells. Consistent with this, in ccRCC and lung adenocarcinoma, but not in lung squamous cell carcinoma, int-FH conferred poor prognosis in patient cohorts. Mb-FH performed its canonical function of complement regulation but had no impact on tumor cell phenotype or patient survival. The discovery of intracellular functions for FH redefines the role of the protein in tumor progression and its use as a prognostic biomarker or potential therapeutic target.

Introduction

The complement cascade is part of the innate immune system [1][2]. Many complement therapeutics are entering clinical trials [3]. Therefore, it is critical to know whether and how complement proteins affect diseases. Tumors are a complement-rich environment [4] in which numerous cell types, including immune cells [5], endothelial cells [6, 7], fibroblasts [8] and the malignant cells themselves [4, 7] contribute to local production of complement components.

Factor H (FH) is the master regulator of C3 convertase, the central enzyme of the complement alternative pathway (AP). Its canonical function is to block C3 convertase formation, enhance C3 convertase dissociation and exert cofactor activity for FI, an enzyme cleaving C3b to inactive fragment iC3b [1]. FH in a tumor can come from the circulation or *in situ* production by tumor cells. Although studies in patients are scarce, animal models and *in vitro* studies reveal that within the tumor microenvironment (TME), FH has context-dependent actions. Overexpression of FH has protumor effects by hampering C3b opsonization and lytic membrane attack complex (MAC) formation on tumor cells [9–11]. Consistent with these observations, injection of a blocking FH antibody reduces lung cancer growth in mice [12]. In contrast, in a mouse model of sarcoma, FH has an antitumoral effect by downregulating the generation of anaphylatoxins, which promote an immunosuppressive environment [13]. Moreover, spontaneous hepatic tumor formation occurs in aged mice with FH deficiency [14].

Not all complement proteins produced by cancer cells are secreted, rather some partially remain within the cell [15]. Intracellular staining of FH (int-FH) is seen in cancer cells in an array of cancer types [10] [16–20], but the function and relevance of this int-FH for tumor progression are poorly understood. In T cells and in pancreatic islets, C3 and/or C5 have intracellular functions unrelated to the complement cascade, these functions are termed non-canonical functions [21–23]. FH also can have roles independent of the complement cascade [19][20][24][25], but it is unclear whether these are related to extracellular or intracellular FH. Considering the diverse, context-dependent and often contradictory modes of action of FH described *in vitro* and in mice, it is critical to assess the role of FH in human cancer if we are to understand its biological functions and shed light on its usefulness as a prognostic biomarker or therapeutic target.

Here, we found that FH was overexpressed by tumor cells in a subset of patients with clear cell renal cell carcinoma (ccRCC) and lung adenocarcinoma (ADC) and was associated with poor prognosis. The protumoral effect of FH resulted from a tumor cell–specific intracellular mode of action that promoted tumor cell proliferation, survival and migration, independent of complement activation.

Materials and methods

Patients

The patients included in this study signed an informed consent. The research was approved by the medical ethics board (N° CEPAR 2014-001, CPP Ile-de-France II n°2016-07-08, n°2008–133 and n°201206–12) and conducted according to the recommendations in the Helsinki Declaration. Primary tumor specimens were collected from 3 retrospective cohorts. The first cohort (cohort 1) was a retrospective cohort of 133 patients with ccRCC who underwent surgery at Institut Mutualiste Montsouris (IMM, Paris, France). The second cohort (cohort 2) included 91 patients with ccRCC whose tumors were collected at the time of surgery at Necker-Enfants Malades Hospital (Paris, France). Cohort 3 consisted in 212 patients with non-small cell lung patients (NSCLC), 112 with ADC and 100 with squamous cell carcinoma (SCC), collected at the Departments of Thoracic Surgery and Pathology of Cochin Hospital, (Paris, France). Plasma samples were collected from a prospective cohort of 61 patients with ccRCC (cohort 4), established at Institut Mutualiste Montsouris (IMM, Paris, France). Histologic subtype of ccRCC or NSCLC, all TNM stages and tissue with good quality for the analysis constituted the inclusion criteria. Histopathologic features such as Fuhrman grade, TNM stages and size were available for most of the patients (Supplementary Table S1). The correlation between FH staining and clinical, histopathological features and immune infiltrate in ccRCC and NSCLC are shown in Supplementary Tables S2 and S3, respectively.

Animal experimentation

C57BL/6J mice were purchased from Charles River Laboratories. HepatoFH$^{-/-}$ mice were generated [26] and provided by Prof. Mathew C. Pickering (Imperial College London, London, UK). The animal experiments were conducted in accordance with the recommendations for the care and use of laboratory animals and with approval l'APAFIS n°3764-201601121739330v3 by the French Ministry of Agriculture. 400,000 mouse TC-1 cells were subcutaneously inoculated in the right flank of the mice in 200 µl PBS. Tumor size was measured with calipers every 2–3 days for 25 days or until reaching 3,000 mm3. Two independent experiments were performed with 5 wild-type (WT) and 5 hepatoFH$^{-/-}$ mice aged 8–10 weeks in experiment 1 and 10 WT and 5 hepatoFH$^{-/-}$ mice in experiment 2.

Immunofluorescence (IF)/immunohistochemistry (IHC)

Formalin-fixed paraffin-embedded (FFPE) human ccRCC or NSCLC specimens were stained for FH, cytokeratin (CK), αSMA, CD31, CD163, CD20, CD3, N-cadherin, E-cadherin, vimentin, calnexin, ACBD5, Golga5, Tom20, PLIN2, Lamp1, C3d, C3c, C3a, cathepsin L, IgG and NaK. The primary and secondary antibodies used, as well as the antigen retrieval and staining conditions, are summarized in Supplementary Table S4. Antigen retrieval was performed with PT-link (Dako PT200) using EnVision FLEX Retrieval Solutions (Dako, pH Low cat. #K8005, pH High cat. #K8004) with high or low pH depending on the antibody. Endogenous peroxidases were then blocked using 3% H_2O_2 (Gilbert, cat. #6553036) solution, followed by blocking of nonspecific staining with Protein Block (Dako, cat. #X0909). The staining was revealed using 3-amino-9-ethylcarbazole substrate (Vector Laboratories, cat. #SK4200). The slides were then counterstained with hematoxylin (Dako, cat. #CS700), mounted with

Glycergel (Dako, cat. #C0563) and scanned with NanoZoomer (Hamamastu). For double staining by IF, a tyramide system was used to avoid species compatibility problems and to increase the fluorescence signal. This system needed an additional step after incubation with the secondary HRP antibody that consisted of an incubation with AF647 tyramide reagent (diluted 1:100 in TBS 1X, H2O2 0.0015%, Life Technologies, cat. #B40958). The entire staining protocol was then repeated for the second primary antibody but with AF546 tyramide reagent (Life Technologies, cat. #B40954). The nuclei were stained with DAPI (ThermoFisher, cat. #62248). The slides were then mounted with Prolong Glass antifade reagent (Invitrogen, cat. #P36980 and scanned with AxioScan (Zeiss). Colocalization between FH and CK was analyzed using HALO Image Analysis software (Indica Labs).

Patient stratification. The antibody Ox24 (which was produced for this study using a hybridoma from ATCC, a kind gift from Pierre Fabre Research Institute) was selected for FH staining. The specificity of Ox24 for FH was validated by staining of liver sections (Geneticist) and inhibition of the signal by pre-incubation with purified FH (Complement Technology, cat. #A317) (Supplementary Figure S1A). Since Ox24 recognizes also Factor H like 1 (FHL-1), a splice variant of FH containing the first 7 domains, the presence of full-length FH in ccRCC tumor sections was validated by additional FH antibodies, the N-terminal–specific antibody Quidel 2 (Quidel, cat. #A254) and antibodies C18 (Abcam, cat. #ab121055) and L20 (ThermoFisher, cat. #GAU-020-03-02), which recognize C-terminal parts of the molecule absent in FHL-1 (Supplementary Figure S1B). For patient stratification, the tumors were classified into 2 groups, high or low, by a semi-quantification method to distinguish the different types of FH staining: int-FH or extracellular (mb-FH). For FH int-FH or mb-FH staining, the high group corresponded to the number of FH-positive cells ≥ 30% and the low group corresponded to that ≤ 30%. Three independent observers (MVD, MR, RT or LTR) performed the analysis to avoid any biases [27]. Automated quantification was not feasible since it was not possible to train the algorithm to reliably distinguish intracellular staining from membrane deposits.

Mouse tumor staining. 6 µm sections of frozen mouse tumor tissues were fixed with cold acetone for 8 minutes and blocked with 5% BSA-TBS for 30 minutes. Tumor sections were then stained with a rabbit polyclonal anti-CD31 (Abcam, cat. #ab124432) or a goat polyclonal antiserum specific for FH (Quidel, cat. #A312) as primary antibodies and then goat anti-rabbit coupled to AF647 (Thermo Fisher Scientific, cat. #A-21245) or donkey anti-goat coupled to AF647 (Thermo Fisher Scientific, cat. #A-21447) as secondary antibodies. The nuclei were stained with DAPI. The slides were then mounted with Prolong Glass antifade reagent and scanned with AxioScan (Zeiss). Quantification of the FH or CD31 staining was analyzed using HALO Image Analysis software (Indica Labs).

Cell lines

Human ccRCC cell lines (Caki-1 and A498), human lung ADC (A549) and SCC (SK-MES) cell lines were purchased from ATCC, in 2016. Primary human umbilical vein endothelial cells (HUVECs) and primary renal proximal tubule cells (RPTECs) were purchased from Lonza in 2016 and 2019, respectively. Caki-1 cells were cultured in McCoy's medium (Gibco, cat. #16600082) + 10% heat-inactivated FCS (Biowest, cat. #S1810-500) + 1X penicillin/streptomycin (Gibco, cat. #10378016). A498 cells were cultured in Eagle minimum essential medium (EMEM) (ATCC, cat. #30-2003) +10% heat-inactivated FCS +1X penicillin/streptomycin. A549 cells were cultured in Dulbecco's modified

eagle medium nutrient mixture F12 (Gibco, cat. #11320033) +10% heat-inactivated FCS +1X penicillin/streptomycin + 1X L-glutamine (Gibco, cat. #25030081) + 1X HEPES (Gibco, cat. #15630080) + 1X non-essential amino-acids solution (Gibco, cat. #11140050). Mouse lung cancer TC-1 cells were a kind gift from Prof. Eric Tartour, INSERM IMRS970, Paris, France and were cultured in RPMI supplemented with 5 mmol/L glutamine (Gibco, cat. #61870036), 10% heat-inactivated FCS, 1× penicillin/streptomycin (Gibco), and 50 μmol/L 2-mercaptoethanol (Gibco, cat. #31350). No specific authentication of the cell lines was performed except comparison of the morphology with the provided images. HUVEC were stained for CD31 and RPTEC for prominin-1 for authentication and found positive. All cell lines were routinely tested for Mycoplasma (Ozyme, cat. #LT07-710) and used only if negative. Primary HUVEC and RPTEC were used for 3 passages, while the tumor cell lines were used for up to 20 passages.

Silencing of *CFH*

The cells were transfected with a preprepared mixture of two siRNAs against *CFH/CFHL-1* at a concentration of 50 nM (Qiagen Hs_CFH_3_Flexitube siRNA, cat. #SI00003983 and Hs_CFH_4_Flexitube siRNA cat. #SI00003990) or siRNA control 50 nM (Qiagen AllStars Negative Control siRNA, cat. #SI03650318, an siRNA with no homology to any known gene sequence) in 5 μL of Lipofectamine RNAiMAX Transfection Reagent (Thermo Fisher, cat. #13778030) in Opti-MEM medium (Gibco, cat. #31985070). After 24 h, the transfection was stopped by changing the Opti-MEM medium to the appropriate medium without antibiotics. The cells were ready to use for the functional experiments 72 h posttransfection. Photos were taken under a microscope 72 h posttransfection to determine the differences in cell number and morphology. The efficiency of the silencing was determined by qRT-PCR and ELISA for cell lysates and supernatants (see below). WT cells correspond to non-transfected cells; siC cells correspond to cells transfected with the control siRNA; siFH cells correspond to cells transfected with CFH siRNA.

Protein extraction

Cells were lysed in RIPA buffer to obtain a total cell lysate. A specific cell fractionation kit (Abcam, cat. #ab109719) was used to prepare the organelles and cytoplasmic and nuclear fractions from cultured cells according to the manufacturer's instructions.

ELISA

FH and C3 concentrations in cell supernatants and cell lysates were measured using a homemade sandwich ELISA [28]. In brief, native antibody (either polyclonal anti-FH (Quidel, cat. #A312) or polyclonal C3 (Calbiochem, cat. #204869)) was coated on a Nunc MaxiSorp ELISA 96-well and 1% PBS-BSA was used for the blocking. Supernatant or cell lysate was added to the plate and incubated for one hour at RT. After washing, the plate was incubated with an in-house biotinylated version of the anti-FH or anti-C3 (biotinylation with EZ link NHS Biotin was performed according to the manufacturer's instructions (Thermo Fisher, cat. #20217) for 1 h at RT. After additional washes, streptavidin coupled with horseradish peroxidase (HRP) (Dako, cat. #P039701-2) was added for 1 h at RT. Binding was revealed using SureBlue TMB Microwell Peroxidase Substrate (Sera Care, cat. #5120-0075), and the reaction was stopped by 2 mol/L sulfuric acid. Multiskan Ex (Thermo Fisher Scientific) was used to

read the optical density at 450 nm. The results are expressed in µg/mL according to the standard curve, made using commercial purified FH or C3 (Complement Technology, cat. #A113).

Western blot

The supernatants or cell lysates of cells cultured without serum for 48 h were recovered and concentrated using Amicon Ultracel 3K units (UFC, cat. #900324). A 10% Bis-Tris gel (Thermo Fisher Scientific) was used to separate the proteins before transfer onto a nitrocellulose membrane. After 1 h of blocking using 5% BSA-TBS, the membrane was incubated overnight at 4°C on a rocking platform with the primary antibodies (Supplementary Table S5) diluted in 5% BSA-TBS. Purified C3 (Calbiochem, cat. #204885), purified C3b (Calbiochem, cat. #204860) and purified iC3b (Calbiochem, cat. #204863) were used as controls. An HRP-conjugated anti-IgG (Supplementary Table S5) was added at 1:1000 dilution for 1 hour at RT under agitation. Visualization was performed by chemiluminescence using a substrate for HRP (SuperSignal WestDuraLuminol, Thermofischer, cat. #1856145) and detected by iBright Western Blot Imaging System (iBright FL1500 Thermofischer).

qRT-PCR

RNA was extracted from the cultured cell lines or from sections of mouse tumors using a Maxwell cell 16 LEV simplyRNA Purification Kit according to the manufacturer's protocol (Promega, cat. #AS1270). The quality and quantity of RNA were determined using the Agilent RNA 6000 Nano Assay kit (cat. #5067-1511) and a 2100 Bioanalyzer (Agilent). An Applied Biosystem High-capacity cDNA Reverse Transcription Kit (Applied Biosystem, cat. #4368814) was used for reverse transcription. Gene expression of C*FH* was assessed by Taqman using primers for human *FH* (ThermoFisher, cat. #Hs00962373_m1) and compared with *GAPDH* (ThermoFisher, cat. #Hs00266705_g1) and *ACTB* (ThermoFisher, cat. #Hs01060665_g1) genes for normalization. Murine gene expression was assessed by Taqman using primers for murine *VEGFA* (ThermoFisher, cat. #Mm00437306_m1), *VEGFB* (ThermoFisher, cat. #Mm00442102_m1), *VEGFC* (ThermoFisher, cat. #Mm00437310_m1), *PECAM-1* (ThermoFisher, cat. #Mm00478712_m1), *FLT4* (ThermoFisher, cat. #Mm01292604_m1), *KDR* (ThermoFisher, cat. #Mm01222421_m1), *PROKR1* (ThermoFisher, cat. #Mm00517546_m1), *VWF* (ThermoFisher, cat. #Mm00550376_m1) and compared with *GAPDH* (ThermoFisher, cat. #Mm01180221_g1) and *ACTB* (ThermoFisher, cat. #Mm02619580_g1) genes for normalization.

RNA-seq

The RNA of 3 independent biological replicates for each condition (siFH vs siC) was used for the RNA-seq study. The libraries were prepared with NEBNext Ultra II Directional RNA Library Prep Kit (New England BioLab, cat. #E7760) according to the manufacturer's protocol: polyA purification using poly-T oligo attached magnetic beads, followed by 300-bp fragmentation with divalent cations under elevated temperature, synthesis of double-stranded cDNA and amplification by PCR. Sequencing was carried out on a paired-end 75 bp Illumina HiSeq 4000 instrument. The quality of FASTQ files was verified using FASTQC and then aligned to a reference genome using STAR tool. Once the data were mapped on the genome, HTSeqCount was used to count and assign reads to a given exon and generate a count table. Before differential analysis, non-expressed genes with a count equal to 0 were removed. The differential expression analysis between siFH and siC was performed using R software and the DESeq2 package

[29]. Results were considered statistically significant at an adjusted p-value of < 0.05. The top 50 most significantly up- or down-regulated genes were sorted by the adjusted p-value; volcano plots were produced, as was a heatmap using heatmap.2 and EnhancedVolcano packages in R. Gene Ontology enrichment analysis was performed with WEV-based Gene SeT AnaLysis Toolkit (WebGestalt) with the GO biological process category. The raw data are available in GEO database under the accession number PRJNA720902.

Flow cytometry

Flow cytometry data were acquired using a BD LSRFortessa X-20 (BD Biosciences) and analyzed using FlowJow software.

C3 deposits. Normal human serum (Etablissement Français du Sang) diluted to 33% in PBS was added to A498, Caki-1, A549 and SK-MES cells for 30 minutes at 37°C with or without a blocking anti-FH (Ox-24). Staining was performed with mouse monoclonal anti-C3c (Quidel, cat. #A205) or isotype control IgG1 (Dako, cat. #X0931) followed by a secondary goat anti-mouse AF700 (Invitrogen, cat. #A-21036).

Proliferation and viability. CFSE reagent 1:1000 (Invitrogen, cat. #C34554) was added to A498, Caki-1, A549 and SK-MES cells for 20 minutes at 37°C. Standard culture medium of each cells was added to stop CFSE staining. Cells were seeded in a 6-well plate and cultured for 72 h in the presence or absence of complete medium supplemented with purified FH at 2 µg/mL or 20 µg/mL. The proliferation capacity of cells was evaluated after the addition of either 50% complete medium or 50% A498 supernatant after 72 h of culture. Supernatants containing dead cells and adherent cells were recovered and stained with DAPI before analysis by flow cytometry.

Cell cycle. After fixation in cold 70% ethanol, 3 µM propidium iodide (PI, Invitrogen, cat. #P1304MP) was added to the cells in the presence of RNase (ThermoFisher, cat. #EN0601) for 15 minutes at RT, in a staining buffer according to the manufacturer's instruction .

FH staining. For int-FH staining, after blocking with 5% BSA, cells were stained with DAPI (1:1000) for 10 minutes at RT. Cells were permeabilized with a BD Cytofix/Cytoperm kit (BD, cat. #554714) or kept non-permeabilized. An FH-specific antibody 1:100 (Quidel, cat. #A224) or mouse isotype control IgG1 was added to cells for 30 minutes at RT. A goat anti-mouse AF488 (Thermo Fisher, cat. #A28175) diluted 1:100 was added after washing.

Immunocytofluorescence

Cells were seeded on a round cover glass and cultured for one day. The adherent cells were fixed with 4% PFA for 30 minutes at RT. Adherent cells were then stained either for actin or NF-κB. A498, Caki-1, HUVEC, RPTEC and SK-MES cells were cultured in their standard culture medium at a confluence of 50-75% then stained for their actin cytoskeleton with Phalloidin-IFluor 488 reagent (Abcam, cat. #ab176753) and with DAPI. A498 were cultured in their standard culture medium at a confluence of 50% before staining for NF-κB, nonspecific staining was blocked by 30min incubation of the cells at RT with Protein Block. Staining was performed with a rabbit monoclonal anti-NF-κB p65 (Cell

Signaling, cat. #8242) and revealed with a goat anti-rabbit coupled with AF647 (Invitrogen, cat. #A21245). Nuclei were stained with DAPI. All stained slides were mounted with Prolong Glass antifade reagent (Thermo Fisher Scientific cat. #P36980) and scanned with AxioScan (Zeiss). The intensity of NF-κB in the nucleus was analyzed on whole slides by using HALO Image Analysis software (Indica Labs).

Migration

To evaluate migration capacity a wound healing assay was performed on cell monolayers of A498, Caki-1, HUVEC and RPTEC cells silenced or not for FH. The monolayers were obtained when cells reached a confluence of 90%, allowing a good monolayer for the twelve next hours. A scratch was generated with a tip, and photographs were taken under a microscope immediately or after 12 hours. The wound healing tool (http://dev.mri.cnrs.fr/projects/imagej-macros/wiki/Wound_Healing_Tool) in ImageJ was used to calculate the percentage of recovery.

Statistical analysis

The package “survival” in R software was used to generate Kaplan-Meier curves, with censoring at 2500 days. A log-rank test was applied to examine the difference between curves. Association between the distributions of two semi-quantitative variables was assessed by the Chi2 test. The difference between siFH and siC cells with regard to proliferation and survival was assessed by the paired T-test; the unpaired T-test is used for cell migration. * $p<0,05$, ** $p<0,01$, *** $p<0,001$, **** $p<0,0001$.

Results

Int-FH but not mb-FH is associated with a negative impact on ccRCC patient survival

In the ccRCC cohort in the TCGA database (KIRC cohort), gene expression of *CFH* above the median was significantly associated with decreased DFS (p=0.03) and OS (p=0.017), suggesting a role of locally produced FH in this type of cancer.

Staining of human ccRCC tumor sections for FH revealed heterogeneous staining patterns by immunohistochemistry (IHC) (**Figure 1**). There were deposits, defined as membranous FH (mb-FH), surrounding the tumor cells and intracellular staining of the tumor cells (int-FH). The mb-FH co-localized with IgG and the NaK ATPase pump by IF (Supplementary Figure S1C,D), suggesting an extracellular location of the mb-FH, corresponding to deposits, which is associated with complement activation [7]. Due to the limitation of the IHC/IF technology, we are not able to firmly conclude that mb-FH is an extracellular deposition of FH at the tumor membrane following complement system activation. Although this seems the most probable explanation, we cannot exclude an intracellular deposit of FH at the internal leaflet of the plasma membrane. FH binds to apoptotic cells, which have a membrane flip-flop, exposing the internal leaflet outside [30, 31]. Therefore, we cannot rule out that some FH present in the cytoplasm could bind to the plasma membrane from inside.

Analysis of the intracellular staining revealed a diffuse coloration of the entire cytoplasm and/or intense granular staining, which was confirmed in consecutive sections using 4 different FH-specific monoclonal antibodies recognizing different epitopes of the molecule (Supplementary Figure S1B). Within the tumor, over 85% of the FH staining localized in tumor cells (cytokeratin) after automatic quantification (Supplementary Figure S2A), confirming the visual observation that tumor cells were the main cells staining positive for FH. Stromal cells, especially fibroblasts, endothelial cells and macrophages were also positive for FH, although to a much lesser extent (Supplementary Figure S2B-D). There was no colocalization of FH with $CD20^+$ B cells or $CD3^+$ T cells (Supplementary Figure S2E-F). The plasma concentration of FH was not different between ccRCC patients and healthy donors (Supplementary Figure S2G), suggesting that FH production by the tumor itself contributes little, if at all, to the plasmatic pool.

To study the specific impact of mb-FH and int-FH, we analyzed tumor tissues obtained from 2 cohorts of ccRCC patients by IHC (Supplementary Table S1). Tumor sections showed different combinations of mb-FH and int-FH staining (Supplementary Figure S3A-D). FH staining at the membrane showed inter-patient and intra-tumoral heterogeneity. These staining patterns allowed us to classify the patients into two groups according to the number of tumor cells carrying FH deposits (**Figure 1A**). In the two ccRCC cohorts, the presence of high or low numbers of tumor cells with FH deposits did significantly not impact survival (cohort 1, DFS, p=0.14; cohort 2, PFS, p=0.226 and OS p=0.627) (**Figure 1B-D**). The same staining heterogeneity was observed for int-FH, and two groups of patients were classified depending on the number of FH-producing cells (**Figure 1E**). Compared to a low density of int-FH^+ cells, a high density of int-FH^+ cells had a negative impact on DFS in cohort 1 (p= 0.00432) (**Figure 1F**) and cohort 2 (PFS: p=0.0274, OS: p=0.0727) (**Figure 1G-H**). The presence of FH inside tumor cells correlated with tumor size, Fuhrman grade and the presence of other complement components,

especially intracellular C4 and C3 (Supplementary Table 2). No association was found between int-FH and the immune infiltrate.

Silencing of FH modifies the transcriptome of ccRCC tumor cells

Since FH was expressed mainly by tumor cells, we confirmed that it was expressed in the ccRCC tumor cell lines A498 (**Figure 2A-C**) and Caki-1 (Supplementary Figure 4A-C). Although these cells lines do not fully recapitulate human RCC [32], they allowed us to explore the role of FH *in vitro*. In both cell lines, FH was detected intracellularly by flow cytometry (**Figure 2A**, Supplementary Figure 4A), and western blotting of the lysate (**Figure 2B**, Supplementary Figure 4B), and was shown to be secreted into the supernatant by ELISA (**Figure 2C**, Supplementary Figure 4D); it was not detected at the cell surface (**Figure 2A**, Supplementary Figure 4A).

We studied the impact of FH on key characteristics of tumor cells using gene silencing. After silencing in A498 and Caki-1 ccRCC cell lines, secretion of FH into the supernatant was reduced by 90–96% and FH in cell lysates was reduced by 85–90% in the cell lysates (**Figure 2D-F,** Supplementary Figure 4B-D). The siRNA-induced silencing of FH revealed a high impact on the phenotype of the ccRCC cells, which acquired a round shape (**Figure 2G,** Supplementary Figure 4E).

To identify the biological processes impacted by FH silencing, RNA-seq was performed on 3 biological replicates for silenced and control A498 and Caki-1 cells. We used $p < 0.05$ and log2-fold change >1 to select the differentially expressed genes. With these criteria, in A498 cells, 235 genes were differentially regulated after FH silencing (**Figure 2H**). Among these genes, 139 were upregulated and 96 were downregulated. For Caki-1 cells, 192 genes were upregulated and 251 were downregulated after FH silencing (Supplementary Figure 4F). We then identified the 50 most differentially expressed genes for each condition (**Figure 2I,** Supplementary Figure 4G). The functional classification analyses of all significantly up- and downregulated genes using the GO "Biological Pathway" categories revealed that these genes were implicated in different biological processes (**Figure 2J,** Supplementary Figure 4H).

Silencing of FH modifies the phenotype of ccRCC tumor cells

RNA-seq analysis revealed an enrichment of genes implicated in cell proliferation in FH-silenced ccRCC cells and a parallel downregulation of genes implicated in the G1/S transition of the mitotic cycle (**Figure 2H–J**). We confirmed that the cell proliferation capacity of FH-silenced A498 cells was significantly reduced in culture (**Figure 3A**). Addition of exogenous FH in the culture medium did not restore the proliferative capacity of FH-silenced A498 ccells or modify the ability of control A498 cells to proliferate (**Figure 3B**). Moreover, the addition of untreated A498 cell supernatant to siFH cells had no effect on their proliferation capacity (**Figure 3C**). These results show that exogenous FH, either purified from plasma or produced by the tumor cells themselves (which may differ from the plasma-derived FH), had no effect on tumor cell proliferation. We therefore conclude that int-FH but not mb-FH is essential for the tumor cell phenotype we observed.

Consistent with the RNA-seq data, we also found that FH-silenced A498 cells were predominantly in the G0-G1 phase (**Figure 3D**). Cell viability was also affected, as indicated by an increase in the number of dead cells when FH was silenced (**Figure 3E**). This could be explained by increased p53 expression (**Figure 3F**). Moreover, FH-silenced A498 cells had a higher percentage of nuclei that stained for NF-κB (**Figure 3G).**

Modifications of genes involved in cell adhesion, extracellular matrix organization and cell morphogenesis were also detected in the RNA-seq analysis (**Figure 2H–J**, Supplementary Figure 4F-H). These transcriptional changes had functional repercussions. FH-silenced A498 cells were rounder with fewer actin filaments and stress fibers (**Figure 3H**). There were also some differentially expressed genes that were involved in cell locomotion and cellular movement. *In vitro*, we confirmed that the migration capacity of FH-silenced A498 cells was decreased, with only 5% scratch recovery at 12 h compared with 40% scratch area recovery for control A498 cells (**Figure 3I, J**). Similar data on proliferation, cell cycle, viability, morphology and subcellular localization of FH were obtained with the Caki-1 cell line (Supplementary Figure 5).

In situ, the more motile cells in a tumor are usually the ones undergoing epithelial to mesenchymal transition (EMT). On ccRCC sections, FH colocalized with tumor cells that had low levels of the epithelial marker cytokeratin (CK) (Supplementary Figure 2A). Increased intensity of CK staining was associated with decreased positivity for FH: cells with low intensity for CK represented 65% of FH^+ cells, whereas tumor cells with medium and high intensity of CK represented only 15% and 5% of FH^+ cells, respectively. In addition, in ccRCC, FH-expressing cells expressed the mesenchymal markers N-cadherin and vimentin (**Figure 3K, L**), suggesting that int-FH is associated with a mesenchymal and hence more motile tumor cell phenotype.

Mb-FH is responsible for complement regulation but has no impact on cellular function

Previous studies indicate that tumor cells produce FH, which can be used as a potential mechanism to escape complement attack [33]. We found that Mb-FH colocalized and correlated with the presence of C3d at the membrane of tumor cells, suggesting that FH is located at the outer leaflet and functions as a complement regulator (**Figure 4A,B**). Compared with siRNA control cells, when FH-silenced A498 or Caki-1 cells were exposed to serum, an increased amount of C3 fragment deposits was observed (**Figure 4C**, Supplementary Figure 6A). Moreover, in the supernatant of the FH-silenced cells, the α43 band corresponding to the inactive fragment of C3b and C3(H2O) (iC3b, iC3(H2O)), was largely undetectable due to loss of factor I (FI) cofactor activity (**Figure 4D,** Supplementary Figure 6B). Indeed, FI was secreted in the supernatants of ccRCC tumor cells (Supplementary Figure 6C). The presence of C3b was detected in only Caki-1 cell supernatant (presence of α' band), but both Caki-1 and A498 cells secreted C3/C3(H2O) (presence of α band). These results indicate that FH silencing results in deregulation of the complement system and an increased level of C3 activation. To decipher whether this overactivation of complement can impact the tumor cell phenotype, we treated A498 cells with the FH blocking antibody Ox-24 at 20 μg/mL, which is in excess compared with the amount of FH secreted. The level of C3 deposits increased when cells were treated with this blocking antibody, reflecting its capacity to

prevent FH binding to C3b and its regulatory function (**Figure 4E**). However, the tumor cell phenotype was not modified, contrary to the condition when cells were silenced for FH (**Figure 4F**), suggesting that extracellular complement regulatory functions had no impact in ccRCC tumor cell phenotype in the tested experimental conditions.

To confirm this *in vivo*, we inoculated TC-1 cells into WT and hepatoFH$^{-/-}$ mice [26]. HepatoFH$^{-/-}$ mice produce only extrahepatic FH and have dramatically reduced FH levels in the circulation (Supplementary Figure 7A). TC-1 expressed very low levels of FH (Supplementary Figure 7B). After hepatoFH$^{-/-}$ mice were inoculated with TC-1 cells, the level of FH inside the tumor was largely decreased (Supplementary Figure 7C, D), meaning that plasma FH is an important source of FH for the tumor. However, tumor growth in hepatoFH$^{-/-}$ mice was not modified compared to that in WT mice (Supplementary Figure 7E). Although FH has been suggested as a neoangiogenesis inhibitor [34], we saw no modification in vascular density or architecture (Supplementary Figure 7F) or angiogenic gene expression in tumors from hepatoFH$^{-/-}$ mice compared with those from WT mice (Supplementary Figure 7G). Thus, plasma FH did not impact tumor growth in this model, which is known to be complement-sensitive [7, 35].

A498 and Caki-1 express C3aR and C5aR1. Therefore, it was possible that the effect of tumor cell–produced FH was related to the control of the autocrine C3a and C5a, generated by the cells themselves. C5a in both untreated and concentrated supernatant was below the detection limit of the ELISA kit [36]. C3a was detected at the limit of the ELISA only in the concentrated supernatant of Caki-1, but was undetectable in A498 [36]. These results are in line with western blotting, where the α' band (corresponding to C3b and indicative of C3a generation) was detected only in the Caki-1 supernatant (**Figure 4D** for A498 and Supplementary Figure 6B for Caki-1). Therefore, even if FH affects local concentrations of C3a and C5a in other contexts, we think this is not a likely mechanism in ccRCC.

Int-FH is localized in lysosomes and interacts with C3

FH silencing resulted in downregulation of genes related to cargo loading on vesicles (**Figure 2J**). In line with this, *in situ* int-FH was located mainly in intracellular vesicles (**Figure 5A**, Supplementary Figure 1C). Fractionation of the different compartments from tumor cells showed that most int-FH was detected in a fraction containing organelles (mitochondria/lysosomes/endoplasmic reticulum/vesicles); very little FH was found in the cytosolic or nuclear compartment (**Figure 5B, C**). Using IF, we identified lysosomes as the organelles containing int-FH (**Figure 5D–I**). C3 is the main partner of FH in the extracellular compartment and has a lysosomal localization in T cells [21]. By cell fractionation, we showed that C3 and FH were located in the same organelles (**Figure 5J**). Furthermore, IF staining with antibodies recognizing epitopes in C3d, C3c or C3a confirmed that FH and C3 were localized in the lysosomes, suggesting an intra-lysosomal interaction (**Figure 5 K–M**). Both FH and C3 can be considered full-length proteins as the staining was detected with different antibodies that detect different domains of FH (**Figure 1A**) and C3 (**Figure 5K–M**). Although C3 can be cleaved by cathepsin L [21] with the help of FH [37], we found that FH and cathepsin L did not colocalize in the ccRCC tumor sections with the limit of our detection method (**Figure 5N**).

The biological effect of FH is specific for tumor cells

Since ccRCC is derived from proximal tubules, we studied FH in this cell type. In peritumoral tissue, we detected areas where some of the proximal tubular cells stained positive for int-FH (**Figure 6A**). Although normal mouse tubules stain positive for FH, in normal human renal tissue the tubules are FH^- and $C3^-$ by the same staining technique we used here [38, 39]. When FH was detected in proximal tubules in ccRCC sections, it colocalized with lysosomes (**Figure 6B**). In primary human renal proximal tubular epithelial cells (RPTECs), we detected FH in the lysate and the supernatant (**Figure 6C**). FH was predominant in the same organelle fraction within these cells as within the tumor cells (**Figure 6D**). Despite efficient FH silencing (**Figure 6E, F**), no modification of the transcriptional program of the cells was observed; only 11 genes were differentially expressed, including *CFH*, between FH-silenced and control RPTECs (**Figure 6G**), compared with 235 genes for A498 cells. Moreover, only 2 differentially expressed genes were common in A498 cells and RPTECs: *CFH* and *NCKAP5*. No effects of FH silencing on the RPTEC phenotype were detected in terms of viability, number of cells or morphology (**Figure 6H**). The actin cytoskeleton of the cells remained the same regardless of whether FH was silenced (**Figure 6I**), and the migration capacity did not change (**Figure 6J**). Even if other parameters may be modified that we did not explore, the effect of FH seems to be specific to tumor cells.

Within the tumor, endothelial cells can produce FH (Supplementary Figure 8A). *In vitro*, endothelial cells (HUVECs) also produce and secrete FH (Supplementary Figure 6B). After efficient silencing (Supplementary Figure 8C-E), no alterations in the phenotype were found in terms of cell number, morphology, actin cytoskeleton and migration capacity (Supplementary Figure 8F-G).

Protumoral effect of int-FH in lung adenocarcinoma

The presence of int-FH^+ cells in tumors was not specific for ccRCC since it was also found in NSCLC tumors (**Figure 7A**). However, Mb-FH was detected only rarely and in small areas of NSCLC tumors (**Figure 7B**). Like ccRCC, the main cell type staining positive for FH was tumor cells (Supplementary Figure 9A), especially mesenchymal tumor cells that expressed high levels of N-cadherin and low levels of E-cadherin (**Figure 7C, D**). Stromal cells such as αSMA^+ fibroblasts and $CD31^+$ endothelial cells also contributed to local production of FH (Supplementary Figure 9B, C). $CD163^+$ macrophages, $CD20^+$ B cells and $CD3^+$ T cells (Supplementary Figure 7D–F) did not stain positive for FH.

To determine whether the protumoral effect of int-FH could be relevant to NSCLC, two cells lines were selected for *in vitro* experiments: A549, a lung ADC cell line, and SK-MES, a lung SCC cell line. A549 cells expressed and secreted equivalent amounts of FH as ccRCC cell lines (**Figure 7E**), whereas SK-MES expressed less (in agreement with [10]). Efficient silencing of FH (**Figure 7F, G**) strongly modified the A549 phenotype (**Figure 7H**) with differences in morphology and proliferation capacity (**Figure 7I**), but without an effect on cell cycle (**Figure 7J**). In contrast, in SK-MES cells, no effects on the phenotype were detected despite efficient FH silencing (Supplementary Figure 8).

Efficient silencing of FH hampered the regulatory activity of FI, preventing C3(H2O) inactivation in the supernatant (**Figure 7K**). No α' band indicative of C3b was detected on the western blot and no C3a or C5a were detected in the supernatant. Upon exposure to normal human serum, FH-silenced A549 cells deposited more complement activation fragments, compared with siRNA control cells (**Figure 7L**). Therefore, FH produced by the A549 cells was functionally active and controlled complement. Since deposits of mb-FH were found only in few patients, survival analysis was not possible.

Int-FH is associated with a poor prognosis value for patients with lung ADC

In NSCLC, we also detected int-FH. The pattern of int-FH staining was the same as that for ccRCC (**Figure 7A**). NSCLC patients with either lung ADC or SCC from cohort 3 (Supplementary Table 1), were classified into two groups according to the number of int-FH^+ cells (**Figure 7M**). In lung ADC, int-FH^+ cells were associated with a negative impact on overall survival (OS) (p=0.0156) (**Figure 7N**). In contrast, in lung SCC, int-FH had no impact on OS (p=0.798) (**Figure 7O**). The negative impact on lung ADC did not correlate with clinical or histological features and did not correlate with the immune infiltrate (Supplementary Table 3).

Discussion

Complement components form a plasma innate immune cascade but also have functions beyond this. Here, we show that FH is locally expressed by multiple types of human tumors. We provide a paradigm shift for the impact of FH on cancer progression, showing what we believe to be a previously unrecognized, likely tumor cell–specific, intracellular function of FH outside the complement cascade (**Figure 7P**). Int-FH served as a driver of the proliferation and migration of ccRCC and lung ADC cells but not of normal cells or lung SCC cells. The presence of int-FH staining in tumor cells indicated poor prognosis for ccRCC and lung ADC.

Prior studies indicate ccRCC and lung ADC are cancers in which complement overactivation occurs and co-regulated overexpression of the genes encoding the complement components as well as detection of C4d in plasma and *in situ* confer poor prognosis [4, 7, 13, 36, 40–44]. Therefore, we were surprised to observe that membranous localization of C3d and FH staining were not associated with prognosis and that int-FH staining and high *CFH* gene expression were associated with decreased survival. Our results echo previous data, where a tendency towards poor prognosis was found in patients with FH^+ tumors in a small cohort of lung ADC [45]. As FH is a key negative complement regulator, one might expect it to control complement cascade activation and reduce C5a, thereby preventing the pro-tumor action of the complement system. In ccRCC, we found that the complement cascade did not proceed to a cytotoxic C5b-9 formation. Therefore, the negative prognostic impact of FH cannot be explained by prevention of complement-mediated tumor cell killing.

Contrary to our expectations, we discovered that the association of FH with poor prognosis was not only a potential biomarker, but also reflected what we believe to be a novel function for FH outside of the complement cascade. Silencing of FH in ccRCC and lung ADC cell lines induced a strong modulation of the tumor cell phenotype, including proliferation, cell cycle, morphology, viability and migration. These results can be explained by the profound modification of the transcriptional program of FH-silenced tumor cell lines, which was marked by alteration in the expression of genes governing the biological processes of adhesion and locomotion. Moreover, within the tumors, int-FH^+ cells were frequently also positive for mesenchymal markers, further suggesting a motile phenotype.

We found that FH was localized mainly within lysosomes. This localization is consistent with the observation that C3 in T cells is in lysosomes, allowing C3a–C3aR interactions and promoting cell survival [21]. FH is stable at low pH (pH 5) [46], suggesting that it can function within this organelle. These findings, together with the alteration of genes involved in cargo loading into vesicles after *CFH* silencing, suggests that int-FH participates in lysosomal trafficking and function. This subcellular location makes it less likely that it serves directly as a transcription factor or regulator of gene expression. In apoptotic cells, FH plays a role as a co-factor for cathepsin L–mediated cleavage of C3 [37]. In ccRCC, int-FH and cathepsin L did not seem to colocalize, suggesting another mode of action. C3 seemed to be in its full length and in its C3(H2O)-like form, due to the low pH in this organelle. The low pH within lysosomes does not seem to be an obstacle for the interaction of C3(H2O) or C3b with int-FH, as they have an optimum at pH 5 [47, 48]. The mechanism by which the tumor cell phenotype is altered by intralysosomal int-FH must be further elucidated. This mode of action is likely different from the one of the intracellular C1s, which also has non-canonical, cascade-unrelated functions in

ccRCC and lung ADC but is localized mainly in the cytoplasm, co-localizing with C4 and cytoplasmic C3 [36].

The reduced proliferation and viability of FH-silenced cells could be explained by cell cycle arrest at G0/G1. At the molecular level, these biological functions could be a consequence of upregulation and phosphorylation of p53, which is a powerful tumor suppressor. P53 arrests cells in G0/G1, reducing survival and controlling proliferation [49]. FH silencing also modified the location of NF-κB within the tumor cells; it became localized predominantly in the nucleus. NF-κB has multiple roles in physiological and pathological processes, promoting or inhibiting apoptosis depending on the context and stimulating gene transcription. Therefore int-FH may contribute to a regulation loop in which p53 and NF-κB participate, especially in cancer [50].

In previous studies, the negative impact of FH on NSCLC was attributed to inhibition of complement activation and protection from complement-mediated tumor cell killing [10, 12, 33, 51–53]. The findings in mouse models of lung cancer, though, are strongly context-dependent and show that complement activation is protumoral [54], antitumoral [12] or irrelevant [6]. Therefore, translating the results frome mouse models to patients is challenging. A limitation of our study is that we could not show in a mouse model that injection of FH-silenced human tumor cell lines reduced tumor growth because the proliferation rate of these cells was so low that we could not generate sufficient numbers to inject the 5 million cells per immunodeficient mouse needed to observe tumor growth in our experimental groups. Nevertheless, our results allow us to conclude that tumor cell–produced FH regulates the complement system, but this process does not seem to have an impact on ccRCC and lung ADC patient survival. Moreover, complement activation in human NSCLC patients is associated with poor prognosis [41, 42], which is consistent with our findings for ccRCC [7]. Additionally, there is no evidence for C5b–9 formation and tumor cell killing in ccRCC and lung ADC in patients. Moreover, in ccRCC patients, the presence of positive staining of membranous C3b/iC3b/C3d is not associated with survival [7] and in lung ADC, FH and C3d deposits are a very rare event. Finally, C5a in the supernatant of the tested cell lines was below the detection limit of the ELISA, suggesting that it is not responsible for the observed effect. Therefore, the canonical action of mb-FH as a complement regulator seems to be less relevant for human lung ADC and ccRCC than the non-canonical action of int-FH. The int-FH action could explain in part why FH-silenced A549 cells showed delayed tumor growth in mice [33].

Outside cancer, FH can also act as an immune regulator by modulating the recruitment and functionality of various immune cell types, such as B cells, monocytes, neutrophils or dendritic cells [55–60] and in breast cancer it promotes recruitment of macrophages and acquisition of an immunosuppressive phenotype [20]. However, in our ccRCC and lung cancer cohorts, no associations were observed between int-FH or mb-FH and immune infiltrate. Therefore, the function of mb-FH in the TME and as a complement regulator is not a major driver of tumor progression in ccRCC and lung cancer.

The *CFH* gene encodes two alternative splice forms: FH and FHL-1. In our study, FH silencing also affected the expression of FHL-1, as previously observed in lung cancer [33] and cSCC [19]. We cannot completely rule out the hypothesis that FHL-1 plays a role in the protumoral effect that we observed. Nevertheless, we found much higher expression of *CFH* within the tumor tissues than *CFHL1*, and absence of the effect of *CFHL-1* on ccRCC patient survival and the use of an shRNA against the C-

terminal part of FH, which does not affect FHL-1, induced the same phenotypic modifications. These data support the conclusion that FH is the main factor responsible for the biological functions altered after *CFH*/*CFHL-1* silencing and that FH, not FHL1, drives tumor progression in ccRCC.

The absence of the effects of FH silencing in RPTECs (from which ccRCC originates) and endothelial HUVECs suggests an oncogenic role. These results do not exclude the possibly that int-FH in other types of normal cells could have a biological function. Indeed, loss of FH impairs antioxidant capacity and energy metabolism of human retinal pigment epithelium cells [34]. In light of our results, the reported impact of the FH Y402H polymorphism, critical for the development of age-related macular degeneration (AMD), on retinal pigment epithelial cell behavior could be explained by the action of int-FH, together with its functions in the microenvironment [61]. This difference between tumor and healthy cells could be explained by differences in the interactome of int-FH or by posttranslational modifications in tumor vs normal cell–derived FH. The int-FH binding partners within the tumor cells remain to be identified. In ovarian cancer, the sialylation level of FH in sera is lower in advanced stage patients than in healthy donors [62]. In hepatocellular carcinoma, enhanced fucosylation of FH is an indicator of premalignant liver disease [63]. In the plasma of lung cancer [12, 51] and AMD [52] patients, FH is detected as a reduced form that displays a decreased C3b binding capacity and a loss of FI cofactor activity [52]. The post translational modifications of FH in ccRCC require further investigation.

It is important to emphasize that FH expression can be pro- or antitumoral according to the cancer type. In hepatocellular carcinoma, high expression of *CFH* is associated with a lower risk of recurrence [64] and high *CFH* is associated with improved survival, whereas *CFH* mutations are associated with worse survival [14]. This may be explained by the fact that FH is mainly produced by the liver and that low FH–expressing tumors will be the ones with the most dedifferentiated cells. Moreover, in addition to cancer organ of origin, our data indicate that the histological subtype is also important to take into account. FH exerted a protumoral effect on lung ADC, but no effects of FH were detected in lung SCC neither patients or in cell lines upon *CFH* silencing. Taken together, these results suggest that therapeutic targeting of FH will be difficult with the conventional antibodies, since the FH blocker has to enter into the cell to be efficient. Moreover, the effect will be context-dependent. Patients with int-FH^+ lung ADC and ccRCC may benefit from int-FH targeting, if such a drug becomes available.

In conclusion, we show that int-FH exerts what we believe to be previously unrecognized functions, including modulation of the transcriptional activity of renal ccRCC and lung ADC cancer cells and effects on their proliferation, cell cycle, morphology and motility. Through these noncanonical functions, rather than through control of complement activation, int-FH confers poor prognosis in these types of cancer.

Acknowledgments

The cytometric and microscopy analyses were performed at the Centre d'Histologie, d'Imagerie et de Cytométrie (CHIC) and the Centre de Recherche des Cordeliers UMRS1138 (Paris, France). We are grateful to the CHIC team for their excellent technical assistance. CHIC is a member of the Université Pierre et Marie Curie Flow Cytometry network (RECYF). We thank the Centre d'Expérimentations

Fonctionnelles team of the Centre de Recherche des Cordeliers for excellent technical assistance and for their support with animal experimentation. We are acknowledging the help from the team of the GenomIC plateform Cochin Institute INSERM U1016 headed by Dr. F. Letourner for the RNA-seq experiments.

Authors' contributions

Designed the study: LTR and MVD. Performed research: MVD, MR, RT, MADD, TRR, CT, NSM, and RN. Analyzed and discussed the data: MVD, MR, RT, MADD, IC, DD, CSF, WHF, and LTR. Provided vital resources: MCP. Provided patient samples and cared for the patients: VV, SMO, AM, PV, XC, RSS, DD, AL, and MA. Wrote the manuscript: MVD, MR, and LTR. All authors read and commented on the manuscript and approved the submission.

References

1. Merle NS, Church SE, Fremeaux-Bacchi V, Roumenina LT (2015) Complement System Part I - Molecular Mechanisms of Activation and Regulation. Front Immunol 6:262. https://doi.org/10.3389/fimmu.2015.00262

2. Merle NS, Noe R, Halbwachs-Mecarelli L, et al (2015) Complement System Part II: Role in Immunity. Front Immunol 6:. https://doi.org/10.3389/fimmu.2015.00257

3. Ricklin D, Mastellos DC, Reis ES, Lambris JD (2018) The renaissance of complement therapeutics. Nat Rev Nephrol 14:26–47. https://doi.org/10.1038/nrneph.2017.156

4. Roumenina L, Daugan MV, Petitprez F, et al (2019) Context-dependent roles of complement in cancer. Nature Reviews Cancer

5. Lubbers R, van Essen MF, van Kooten C, Trouw LA (2017) Production of complement components by cells of the immune system. Clin Exp Immunol 188:183–194. https://doi.org/10.1111/cei.12952

6. Bulla R, Tripodo C, Rami D, et al (2016) C1q acts in the tumour microenvironment as a cancer-promoting factor independently of complement activation. Nature Communications 7:10346. https://doi.org/10.1038/ncomms10346

7. Roumenina LT, Daugan MV, Noé R, et al (2019) Tumor Cells Hijack Macrophage-Produced Complement C1q to Promote Tumor Growth. Cancer Immunol Res. https://doi.org/10.1158/2326-6066.CIR-18-0891

8. Al-Adnani MS, McGEE JO (1976) C1q production and secretion by fibroblasts. Nature 263:145–146. https://doi.org/10.1038/263145a0

9. Kesselring R, Thiel A, Pries R, et al (2014) The complement receptors CD46, CD55 and CD59 are regulated by the tumour microenvironment of head and neck cancer to facilitate escape of complement attack. Eur J Cancer 50:2152–2161. https://doi.org/10.1016/j.ejca.2014.05.005

10. Ajona D, Castaño Z, Garayoa M, et al (2004) Expression of complement factor H by lung cancer cells: effects on the activation of the alternative pathway of complement. Cancer Res 64:6310–6318. https://doi.org/10.1158/0008-5472.CAN-03-2328

11. Fishelson Z, Kirschfink M (2019) Complement C5b-9 and Cancer: Mechanisms of Cell Damage, Cancer Counteractions, and Approaches for Intervention. Front Immunol 10:752. https://doi.org/10.3389/fimmu.2019.00752

12. Bushey RT, Moody MA, Nicely NL, et al (2016) A Therapeutic Antibody for Cancer, Derived from Single Human B Cells. Cell Rep 15:1505–1513. https://doi.org/10.1016/j.celrep.2016.04.038

13. Bonavita E, Gentile S, Rubino M, et al (2015) PTX3 is an extrinsic oncosuppressor regulating complement-dependent inflammation in cancer. Cell 160:700–714. https://doi.org/10.1016/j.cell.2015.01.004

14. Laskowski J, Renner B, Pickering MC, et al (2020) Complement factor H–deficient mice develop spontaneous hepatic tumors. J Clin Invest 130:. https://doi.org/10.1172/JCI135105

15. Arbore G, Kemper C, Kolev M (2017) Intracellular complement - the complosome - in immune cell regulation. Mol Immunol 89:2–9. https://doi.org/10.1016/j.molimm.2017.05.012

16. Junnikkala S, Hakulinen J, Jarva H, et al (2002) Secretion of soluble complement inhibitors factor H and factor H-like protein (FHL-1) by ovarian tumour cells. British Journal of Cancer 87:1119. https://doi.org/10.1038/sj.bjc.6600614

17. Gasque P, Julen N, Ischenko AM, et al (1992) Expression of complement components of the alternative pathway by glioma cell lines. J Immunol 149:1381–1387

18. Junnikkala S, Jokiranta TS, Friese MA, et al (2000) Exceptional resistance of human H2 glioblastoma cells to complement-mediated killing by expression and utilization of factor H and factor H-like protein 1. J Immunol 164:6075–6081. https://doi.org/10.4049/jimmunol.164.11.6075

19. Riihilä PM, Nissinen LM, Ala-Aho R, et al (2014) Complement factor H: a biomarker for progression of cutaneous squamous cell carcinoma. J Invest Dermatol 134:498–506. https://doi.org/10.1038/jid.2013.346

20. Smolag KI, Mueni CM, Leandersson K, et al (2020) Complement inhibitor factor H expressed by breast cancer cells differentiates CD14+ human monocytes into immunosuppressive macrophages. OncoImmunology 9:1731135. https://doi.org/10.1080/2162402X.2020.1731135

21. Liszewski MK, Kolev M, Le Friec G, et al (2013) Intracellular Complement Activation Sustains T Cell Homeostasis and Mediates Effector Differentiation. Immunity 39:1143–1157. https://doi.org/10.1016/j.immuni.2013.10.018

22. West EE, Kolev M, Kemper C (2018) Complement and the Regulation of T Cell Responses. Annual Review of Immunology 36:309–338. https://doi.org/10.1146/annurev-immunol-042617-053245

23. King BC, Kulak K, Krus U, et al (2019) Complement Component C3 Is Highly Expressed in Human Pancreatic Islets and Prevents β Cell Death via ATG16L1 Interaction and Autophagy Regulation. Cell Metab 29:202-210.e6. https://doi.org/10.1016/j.cmet.2018.09.009

24. Józsi M, Schneider AE, Kárpáti É, Sándor N (2019) Complement factor H family proteins in their non-canonical role as modulators of cellular functions. Seminars in Cell & Developmental Biology 85:122–131. https://doi.org/10.1016/j.semcdb.2017.12.018

25. Seol HS, Lee SE, Song JS, et al (2016) Complement proteins C7 and CFH control the stemness of liver cancer cells via LSF-1. Cancer Lett 372:24–35. https://doi.org/10.1016/j.canlet.2015.12.005

26. Vernon KA, Ruseva MM, Cook HT, et al (2016) Partial Complement Factor H Deficiency Associates with C3 Glomerulopathy and Thrombotic Microangiopathy. J Am Soc Nephrol 27:1334–1342. https://doi.org/10.1681/ASN.2015030295

27. Daugan MV, Revel M, Lacroix L, et al (2021) Complement Detection in Human Tumors by Immunohistochemistry and Immunofluorescence. Methods Mol Biol 2227:191–203. https://doi.org/10.1007/978-1-0716-1016-9_18

28. Dragon-Durey M-A, Frémeaux-Bacchi V, Loirat C, et al (2004) Heterozygous and homozygous factor h deficiencies associated with hemolytic uremic syndrome or membranoproliferative glomerulonephritis: report and genetic analysis of 16 cases. J Am Soc Nephrol 15:787–795. https://doi.org/10.1097/01.asn.0000115702.28859.a7

29. Love MI, Huber W, Anders S (2014) Moderated estimation of fold change and dispersion for RNA-seq data with DESeq2. Genome Biology 15:550. https://doi.org/10.1186/s13059-014-0550-8

30. Trouw LA, Bengtsson AA, Gelderman KA, et al (2007) C4b-binding Protein and Factor H Compensate for the Loss of Membrane-bound Complement Inhibitors to Protect Apoptotic Cells against Excessive Complement Attack *. Journal of Biological Chemistry 282:28540–28548. https://doi.org/10.1074/jbc.M704354200

31. Leffler J, Herbert AP, Norström E, et al (2010) Annexin-II, DNA, and histones serve as factor H ligands on the surface of apoptotic cells. J Biol Chem 285:3766–3776. https://doi.org/10.1074/jbc.M109.045427

32. Lovell M, Lott ST, Wong P, et al (1999) The Genetic Locus NRC-1 within Chromosome 3p12 Mediates Tumor Suppression in Renal Cell Carcinoma Independently of Histological Type, Tumor Microenvironment, and VHL Mutation. Cancer Res 59:2182–2189

33. Ajona D, Hsu Y-F, Corrales L, et al (2007) Down-Regulation of Human Complement Factor H Sensitizes Non-Small Cell Lung Cancer Cells to Complement Attack and Reduces In Vivo Tumor Growth. The Journal of Immunology 178:5991–5998. https://doi.org/10.4049/jimmunol.178.9.5991

34. Liu J, Hoh J (2017) Loss of Complement Factor H in Plasma Increases Endothelial Cell Migration. J Cancer 8:2184–2190. https://doi.org/10.7150/jca.19452

35. Markiewski MM, DeAngelis RA, Benencia F, et al (2008) Modulation of the antitumor immune response by complement. Nat Immunol 9:1225–1235. https://doi.org/10.1038/ni.1655

36. Daugan MV, Revel M, Russick J, et al (2021) Complement C1s and C4d as prognostic biomarkers in renal cancer: emergence of non-canonical functions of C1s. Cancer Immunol Res

37. Martin M, Leffler J, Smoląg KI, et al (2016) Factor H uptake regulates intracellular C3 activation during apoptosis and decreases the inflammatory potential of nucleosomes. Cell Death Differ 23:903–911. https://doi.org/10.1038/cdd.2015.164

38. Boudhabhay I, Poillerat V, Grunenwald A, et al (2020) Complement activation is a crucial driver of acute kidney injury in rhabdomyolysis. Kidney Int. https://doi.org/10.1016/j.kint.2020.09.033

39. Merle NS, Leon J, Poillerat V, et al (2020) Circulating FH Protects Kidneys From Tubular Injury During Systemic Hemolysis. Front Immunol 11:1772. https://doi.org/10.3389/fimmu.2020.01772

40. Corrales L, Ajona D, Rafail S, et al (2012) Anaphylatoxin C5a creates a favorable microenvironment for lung cancer progression. J Immunol 189:4674–4683. https://doi.org/10.4049/jimmunol.1201654

41. Ajona D, Pajares MJ, Corrales L, et al (2013) Investigation of complement activation product c4d as a diagnostic and prognostic biomarker for lung cancer. J Natl Cancer Inst 105:1385–1393. https://doi.org/10.1093/jnci/djt205

42. Ajona D, Okrój M, Pajares MJ, et al (2017) Complement C4d-specific antibodies for the diagnosis of lung cancer. Oncotarget 9:6346–6355. https://doi.org/10.18632/oncotarget.23690

43. Reese B, Silwal A, Daugherity E, et al (2020) Complement as Prognostic Biomarker and Potential Therapeutic Target in Renal Cell Carcinoma. J Immunol 205:3218–3229. https://doi.org/10.4049/jimmunol.2000511

44. Motzer RJ, Banchereau R, Hamidi H, et al (2020) Molecular Subsets in Renal Cancer Determine Outcome to Checkpoint and Angiogenesis Blockade. Cancer Cell 38:803-817.e4. https://doi.org/10.1016/j.ccell.2020.10.011

45. Cui T, Chen Y, Knösel T, et al (2011) Human complement factor H is a novel diagnostic marker for lung adenocarcinoma. Int J Oncol 39:161–168. https://doi.org/10.3892/ijo.2011.1010

46. Okemefuna AI, Nan R, Gor J, Perkins SJ (2009) Electrostatic interactions contribute to the folded-back conformation of wild type human factor H. J Mol Biol 391:98–118. https://doi.org/10.1016/j.jmb.2009.06.010

47. Sim E, Sim RB (1983) Enzymic assay of C3b receptor on intact cells and solubilized cells. Biochemical Journal 210:567–576. https://doi.org/10.1042/bj2100567

48. Kask L, Villoutreix BO, Steen M, et al (2004) Structural stability and heat-induced conformational change of two complement inhibitors: C4b-binding protein and factor H. Protein Sci 13:1356–1364. https://doi.org/10.1110/ps.03516504

49. Kastenhuber ER, Lowe SW (2017) Putting p53 in Context. Cell 170:1062–1078. https://doi.org/10.1016/j.cell.2017.08.028

50. Carrà G, Lingua MF, Maffeo B, et al (2020) P53 vs NF-κB: the role of nuclear factor-kappa B in the regulation of p53 activity and vice versa. Cell Mol Life Sci 77:4449–4458. https://doi.org/10.1007/s00018-020-03524-9

51. Campa MJ, Gottlin EB, Bushey RT, Patz EF (2015) Complement Factor H Antibodies from Lung Cancer Patients Induce Complement-Dependent Lysis of Tumor Cells, Suggesting a Novel

Immunotherapeutic Strategy. Cancer Immunol Res 3:1325–1332. https://doi.org/10.1158/2326-6066.CIR-15-0122

52. Krilis M, Qi M, Qi J, et al (2018) Dual roles of different redox forms of complement factor H in protecting against age related macular degeneration. Free Radic Biol Med 129:237–246. https://doi.org/10.1016/j.freeradbiomed.2018.09.034

53. Amornsiripanitch N, Hong S, Campa MJ, et al (2010) Complement factor H autoantibodies are associated with early stage NSCLC. Clin Cancer Res 16:3226–3231. https://doi.org/10.1158/1078-0432.CCR-10-0321

54. Kwak JW, Laskowski J, Li HY, et al (2018) Complement Activation via a C3a Receptor Pathway Alters CD4+ T Lymphocytes and Mediates Lung Cancer Progression. Cancer Res 78:143–156. https://doi.org/10.1158/0008-5472.CAN-17-0240

55. Tsokos GC, Inghirami G, Tsoukas CD, et al (1985) Regulation of immunoglobulin secretion by factor H of human complement. Immunology 55:419–426

56. Nabil K, Rihn B, Jaurand MC, et al (1997) Identification of human complement factor H as a chemotactic protein for monocytes. Biochem J 326 (Pt 2):377–383. https://doi.org/10.1042/bj3260377

57. Ohtsuka H, Imamura T, Matsushita M, et al (1993) Thrombin generates monocyte chemotactic activity from complement factor H. Immunology 80:140–145

58. Olivar R, Luque A, Cárdenas-Brito S, et al (2016) The Complement Inhibitor Factor H Generates an Anti-Inflammatory and Tolerogenic State in Monocyte-Derived Dendritic Cells. The Journal of Immunology 196:4274–4290. https://doi.org/10.4049/jimmunol.1500455

59. Dixon KO, O'Flynn J, Klar-Mohamad N, et al (2017) Properdin and factor H production by human dendritic cells modulates their T-cell stimulatory capacity and is regulated by IFN-γ. Eur J Immunol 47:470–480. https://doi.org/10.1002/eji.201646703

60. Schneider AE, Sándor N, Kárpáti É, Józsi M (2016) Complement factor H modulates the activation of human neutrophil granulocytes and the generation of neutrophil extracellular traps. Molecular Immunology 72:37–48. https://doi.org/10.1016/j.molimm.2016.02.011

61. Hallam D, Collin J, Bojic S, et al (2017) An Induced Pluripotent Stem Cell Patient Specific Model of Complement Factor H (Y402H) Polymorphism Displays Characteristic Features of Age-Related Macular Degeneration and Indicates a Beneficial Role for UV Light Exposure. Stem Cells 35:2305–2320. https://doi.org/10.1002/stem.2708

62. Wu J, Xie X, Nie S, et al (2013) Altered expression of sialylated glycoproteins in ovarian cancer sera using lectin-based ELISA assay and quantitative glycoproteomics analysis. J Proteome Res 12:3342–3352. https://doi.org/10.1021/pr400169n

63. Benicky J, Sanda M, Pompach P, et al (2014) Quantification of fucosylated hemopexin and complement factor H in plasma of patients with liver disease. Anal Chem 86:10716–10723. https://doi.org/10.1021/ac502727s

64. Yang JD, Seol S-Y, Leem S-H, et al (2011) Genes associated with recurrence of hepatocellular carcinoma: integrated analysis by gene expression and methylation profiling. J Korean Med Sci 26:1428–1438. https://doi.org/10.3346/jkms.2011.26.11.1428

Figure Legends

Figure 1: Int-FH produced by tumor cells, not mb-FH, is associated with poor prognosis in ccRCC.

A) Presence of FH deposits (mb-FH) at the membrane of tumor cells by IHC on paraffin-embedded ccRCC sections. The tumors were classified into 2 groups: high or low. High was defined as over 30% of FH^+ tumor cells and low as less than 30% of FH^+ tumor cells. **B)** Kaplan-Meier curve of disease-free survival (DFS) according to the high/low classification for FH deposits (mb-FH) in ccRCC cohort 1. **C-D)** Kaplan-Meier curves of progression-free survival (PFS) and overall survival (OS) according to the high/low classification for FH deposits (mb-FH) in ccRCC cohort 2. **E)** Presence of FH within the cytoplasm of tumor cells (int-FH) by IHC on paraffin-embedded ccRCC sections. The tumors were classified into 2 groups: high or low. High was defined as over 30% of FH^+ tumor cells and low as less than 30% of FH^+ tumor cells. **F)** Kaplan-Meier curve of DFS according to the high/low classification for int-FH in ccRCC cohort 1. **G-H)** Kaplan-Meier curves of PFS and OS according to the high/low classification for int-FH in ccRCC cohort 2. For all Kaplan-Meier curves (**B–D** and **F–H**), a log-rank test was used, and $p<0.05$ was considered significant.

Figure 2: FH silencing modifies the ccRCC tumor cell transcriptome

A) Histogram representing FH staining in A498 ccRCC cells: extracellular FH (no permeabilization step), red = isotype (ISO), blue = FH; intracellular FH (with permeabilization step), orange = isotype (ISO), green = FH. **B)** Western blot of FH in the supernatant of A498 cells (siFH, siC) under non-reducing conditions. **C)** FH concentration in the lysate (n=2) and the supernatant (n=5) of A498 cell lines determined by ELISA, error bars represent mean with SD. **D)** FH concentration in the supernatant of A498 cells (siFH n=5, siC n=6, WT n=4) determined by ELISA. **E)** FH concentration in the lysate of A498 cells (siFH n=2, siC n=2) determined by ELISA. **F)** FH expression by A498 cells (siFH n=2, siC n=2) determined by qRT-PCR. **G)** General aspect of the RPTEC cells post FH silencing. Images (100x) of A498 cells 72 h post-transfection with siFH or siC. **F-J)** Transcriptomic analyses (RNAseq) of A498 after silencing of FH. **H)** Volcano plot depicting the results of differential expression obtained with DESeq2 analysis between A498 siFH (n=3) and A498 siC cells (n=3). The volcano plot was generated with R software and the EnhancedVolcano package. Red points represent genes with a log2-fold change >1 and Padj< 0.05. **I)** Heatmap of log2 counts for the top 50 differentially expressed genes after silencing A498 cells with siFH vs siC. The most differentially expressed genes were selected on the adjusted p-value. Expression across each gene was row scaled, with relatively high expression of a given gene marked in red and samples with relatively low expression marked in blue. Lighter shades and white represent genes with intermediate expression levels. **J)** GO analysis of functional annotations (biological process) up- or downregulated by FH silencing vs. A498 siC

Figure 3: FH silencing modifies ccRCC tumor cell phenotype

A–C) Evaluation of proliferation of A498 cells after FH silencing. **A)** Fold change in CFSE geometric means in A498 siFH vs. A498 siC cells in 4 independent experiments, ** $p<0.01$. **B)** Histogram representing CFSE intensity on A498 siFH or A498 siC cells with or without 2 µg/mL purified FH after 72 h of proliferation (purple = unstained A498 cells; blue = A498 taken at the time of CFSE staining [T0]; dark green = A498 siC cells; light green = A498 siC cells + purified FH; red= A498 siFH cells; and orange = A498 siFH cells + purified FH). **C)** Histogram representing CFSE intensity on A498 siFH or A498 siC cells with or without the addition of A498 cell supernatant after 72 h of proliferation (purple = unstained A498 cells; blue = A498 cells taken at the time of CFSE staining [T0]; dark green = A498 siC cells; light green = A498 siC cells + A498 supernatant; red= A498 siFH cells; and orange = A498 siFH cells + A498 supernatant). **D)** Percentage of cells in each cell cycle phase (G0-G1/S/G2-M) determined by flow cytometry analysis of PI staining of A498 siFH or siC cells in four independent experiments, * $p<0.05$. **E)** Evaluation of viability by measuring the percentage of $DAPI^+$ dead cells by flow cytometry after 72 h of culture in A498 siFH or A498 siC cells in five independent experiments, ** $p<0.01$**. F)** Western blot analysis of the A498 siFH or siC cell lysate for p53, p53 S15 and p53 S46. **G)** Quantification by HALO software of the percentage of WT, siC or siFH cells according to the intensity of NFkB staining (negative, low, medium and high), in two independent experiments, error bars represent mean with SD. **H)** Cell morphology evaluated by IF staining of phalloïdin (red) in A498 siFH (right) or siC (left). **I)** Analysis of the migration capacity of A498 siFH cells and A498 siC cells. A scratch on the A498 monolayer was made at T0, and a photo of the scratch area was taken. After 12 h, a photo of the same area was taken to compare the migration capacity. **J)** An ImageJ wound healing macro was used to determine the area of the scratch at each time point. The percentage of closing of the scratch area was calculated with the following calculation: 100-(scratch area T0/scratch area t+12h), **** $p<0.0001$, error bars represent mean with SD. **K–L)** Int-FH is associated with markers of epithelial to mesenchymal transition in NSCLC. **K)** Double staining by IF of FH (green) and Ncad (red) on paraffin-embedded ccRCC sections. **L)** Double staining by IF of FH (green) and Vimentin (red) on paraffin-embedded ccRCC sections.

Figure 4: Mb-FH regulates complement on tumor cells but does not impact the cell phenotype. A) Double staining by IF of FH (green) and C3d (red) on paraffin-embedded ccRCC sections. **B)** Histogram representing the correlation between FH deposits (mb-FH) on tumor cells and C3d deposits (C3d D) from cohort 2. The association was calculated by using a χ^2 test, and Ch2 $p<0.05$ was considered significant. **C–F)** FH produced by A498 cells retains complement-regulatory activity but has no impact on cell phenotype. **C)** C3 deposits on the A498 cell surface after incubation with NHS determined by flow cytometry (red: isotype control [ISO], blue: A498 siC, orange: A498 siFH). **D)** Western blot for C3 in reducing conditions in the supernatant of A498 siFH and A498 siC cells. **E)** C3 deposits on the A498 cell surface after incubation with NHS in the presence or absence of 20 µg/mL FH blocking antibody (Ox-24), as determined by flow cytometry (red: isotype control, green: A498 treated with ox-

24, orange: A498 ST). **F)** Images (100x) of A498 cells 72 h posttransfection with siFH or siC or after treatment with Ox-24.

Figure 5: Int-FH is located in lysosomes and interacts with C3.

A) FH staining by IF of FH (green) on paraffin-embedded ccRCC sections **B)** FH quantification by ELISA on the subcellular fraction of A498 cells (cytoplasmic, organelle and nuclear), in 3 independent experiments, error bars represent mean with SD. **C)** Western blot for FH in nonreducing conditions in the lysate of the cell fractions of A498 cells: cytoplasmic, organelles and nuclear fractions. **D–I)** Double staining by IF on paraffin-embedded ccRCC sections. **D)** calnexin (green) for endoplasmic reticulum and FH (red). **E)** ACBD5 (red) for peroxisomes and FH (green). **F)** GOLGA5 (red) for Golgi apparatus and FH (green). **G)** Tom20 (red) for mitochondria and FH (green). **H)** PLIN2 (red) for lipid droplet and FH (green). **I)** Lamp1 (green) for lysosomes and FH (red). **J)** FH quantification by ELISA on the subcellular fraction of A498 cells (cytoplasmic, organelle and nuclear), in 3 independent experiments, error bars represent mean with SD. **K–N)** Double staining by IF on paraffin-embedded ccRCC sections. **K)** C3d (green) and FH (red). **L)** C3c (green) and FH (red). **M)** C3a (green) and FH (red). **N)** cathepsin L (green) and FH (red).

Figure 6: Silencing FH in RPTECs had no impact on the transcriptome and the phenotype.

A) FH staining of tubular cells in peritumoral tissue by IHC. **B)** Double staining by IF on paraffin-embedded ccRCC sections of FH (green) with calnexin (red) for endoplasmic reticulum, Tom20 (red) for mitochondria and Lamp1 (green) for lysosomes. **C)** FH concentration in the lysate and the supernatant of RPTECs determined by ELISA. **D)** FH quantification by ELISA on the subcellular fractions of RPTECs (cytoplasmic, organelle and nuclear). **E)** FH concentration in the supernatant of RPTECs (siFH, siC) determined by ELISA. **F)** FH concentration in the lysate of RPTECs (siFH, siC) determined by ELISA. **G)** Transcriptomic analyses of RPTEC, silenced or not for FH. Heatmap of log2 counts for differentially expressed genes after silencing RPTECs with siFH vs siC. Expression across each gene has been row scaled, with relatively high expression of a given gene marked in red and samples with relatively low expression marked in blue. Lighter shades and white represent genes with intermediate expression levels. **H)** General aspect of the RPTEC cells post FH silencing. Images (100x) of RPTECs 72 h posttransfection with siFH or siC. **I)** Immunofluorescence staining of phalloïdin (red) in siFH (right) or siC (left) RPTECs. **J)** Analysis of the migration capacity of siFH RPTECs and siC RPTECs. A scratch on the RPTEC monolayer was made at T0, and a photo of the scratch area was taken. After 12 h, a photo of the same area was taken to compare the migration capacity. An ImageJ wound healing macro was used to determine the area of the scratch at each time point. The percentage of closing of the scratch area was calculated with the following calculation: 100-(scratch area T0/scratch area t+12h), in 3 independent experiments, error bars represent mean with SD.

Figure 7: Int-FH but not mb-FH exerts a protumoral effect on lung adenocarcinoma.

A) Image of Int-FH staining by IHC on paraffin-embedded NSCLC sections. **B)** Image of Mb-FH staining by IHC on paraffin-embedded NSCLC sections. **C–D)** Int-FH is associated with markers of

epithelial to mesenchymal transition in lung ADC. **C)** Double staining by IF of FH (green) and Ecad (red) on paraffin-embedded lung ADC sections. **D)** Double staining by IF of FH (green) and Ncad (red) on paraffin-embedded lung ADC sections. **E)** FH concentration in the lysate and the supernatant of lung ADC cell line A549, determined by ELISA, in 2 independent experiments, error bars represent mean with SD. **F)** FH concentration in the supernatant of A549 cells (siFH, siC, WT) determined by ELISA, * $p<0.05$, in 3 independent experiments, error bars represent mean with SD. **G)** Western blot of FH in the supernatant of A549 cells (siFH, siC) under nonreducing conditions. **H–J)** FH silencing modifies the phenotype of A549 cells. **H)** General aspect of the A549 cells after FH silencing. Images (100x) of A549 cells 72 h posttransfection with siFH or siC. **I)** Evaluation of proliferation of A549 cells after FH silencing. Histogram representing CFSE intensity on A549 siFH or A549 siC cells after 72 h of proliferation (green = unstained A549 cells; orange = A549 cells taken at the time of CFSE staining [T0]; red = A549 siC cells after 72 h of proliferation; blue = A549 siFH cells after 72 h of proliferation). **J)** Percentage of cells in each cell cycle phase (G0-G1/S/G2-M) determined by flow cytometry analysis of PI staining on A549 siFH or siC cells in four independent experiments. **K–L)** FH produced by A549 cells regulates complement. **K)** Complement-regulatory activity of FH produced by A549 cells. Western blot for C3 in reducing conditions in the supernatant of A549 siFH and A549 siC cells. **L)** C3 deposits on the A549 cell surface after incubation with NHS determined by flow cytometry (green: isotype control cells, red: A549 siC cells, blue: A549 siFH cells). **M)** Classification of NSCLC tumors according to the presence of FH within the cytoplasm of tumor cells by IHC. The tumors were classified into 2 groups: high or low. High was defined as over 30% of FH^+ cells and low as less than 30% of FH^+ cells. **N–O)** Kaplan-Meier curves for OS according to the high/low classification for int-FH in NSCLC cohort 3. **N)** Lung ADC. **O)** Lung SCC. A log-rank test was used, and $p<0.05$ was considered significant **P)** Proposed mode of action of FH in the TME and within the tumor cell.

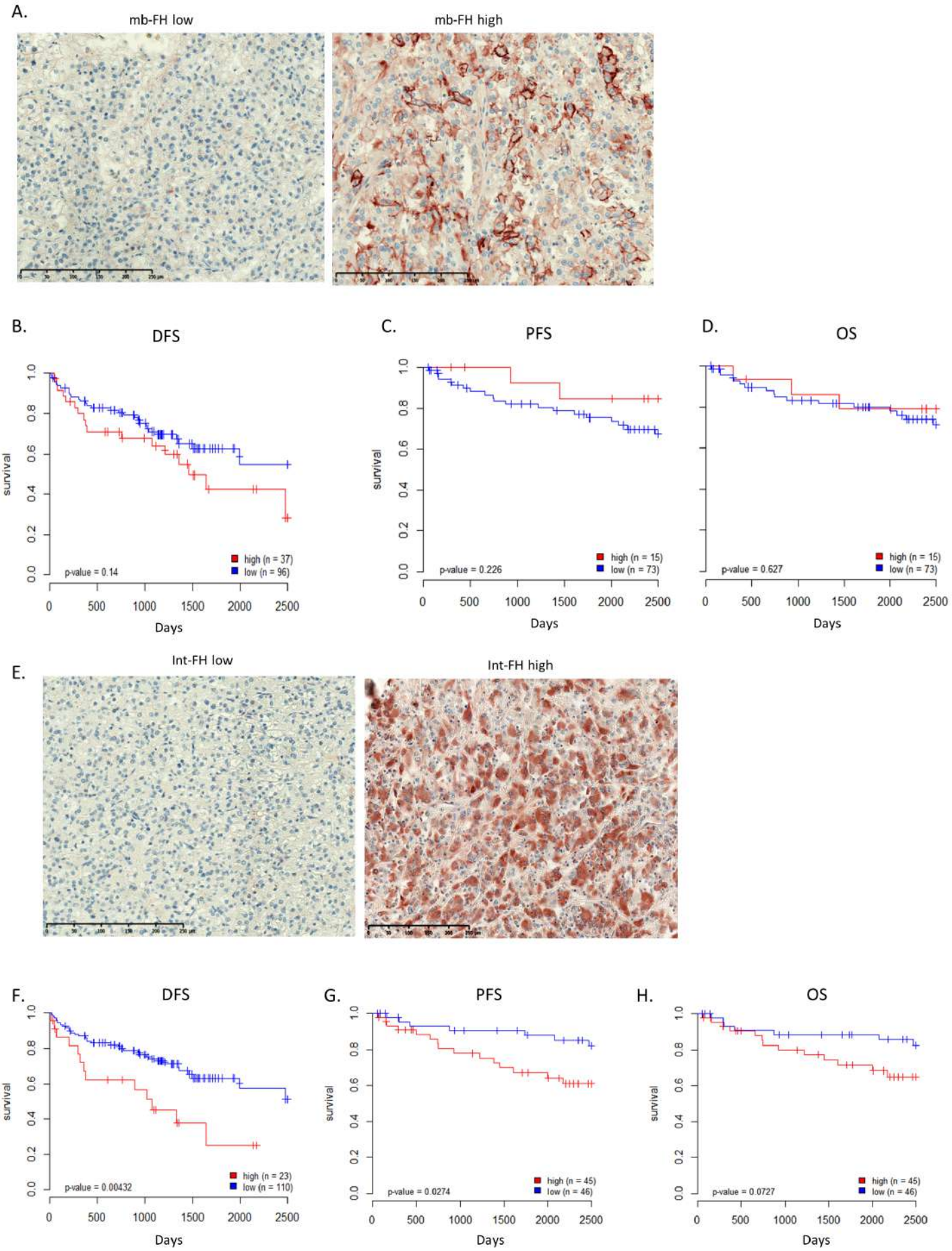

Figure 1: Int-FH produced by tumor cells but not mb-FH is associated with poor prognosis in ccRCC..

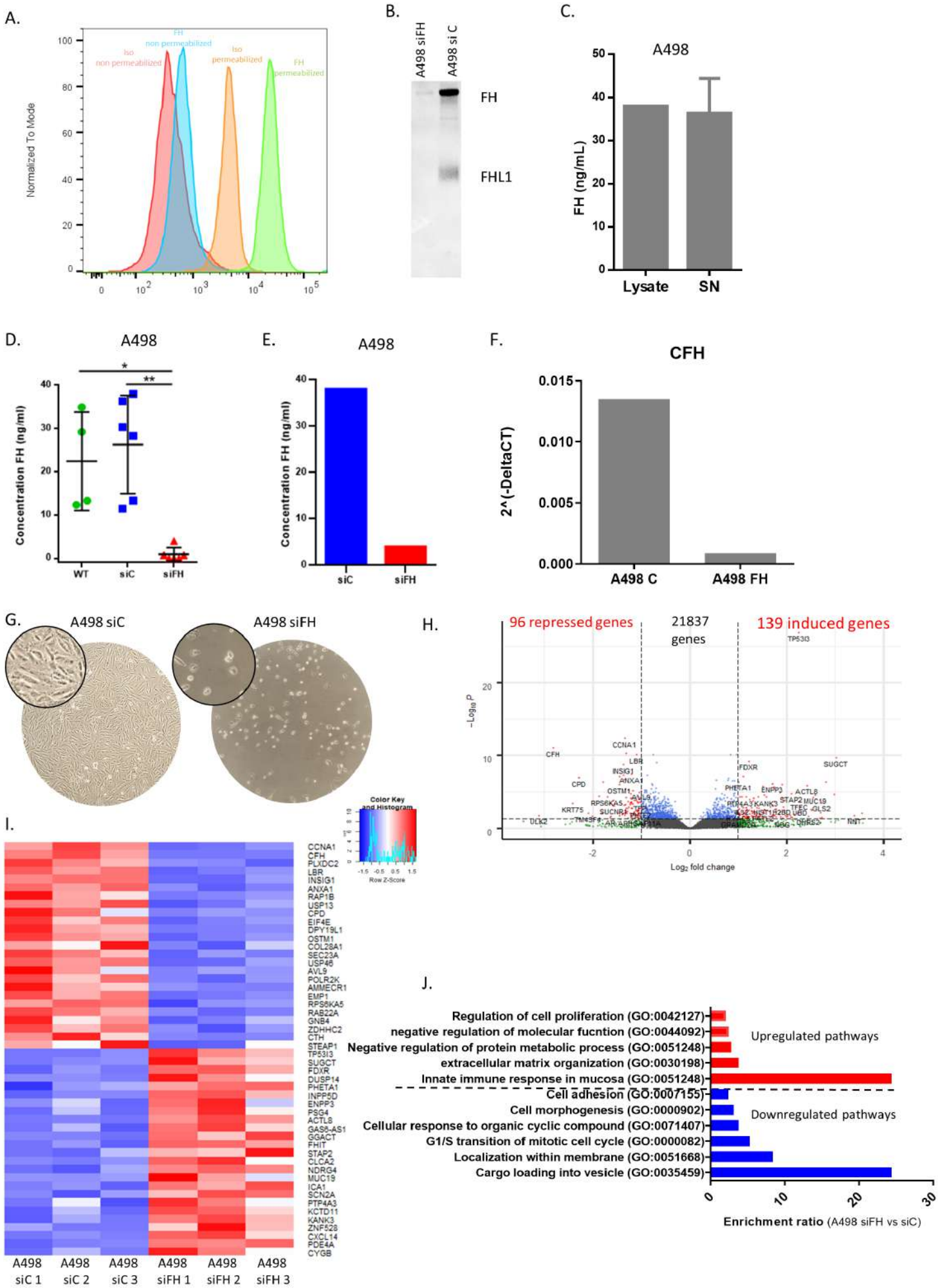

Figure 2: FH silencing modifies ccRCC tumor cell transcriptome

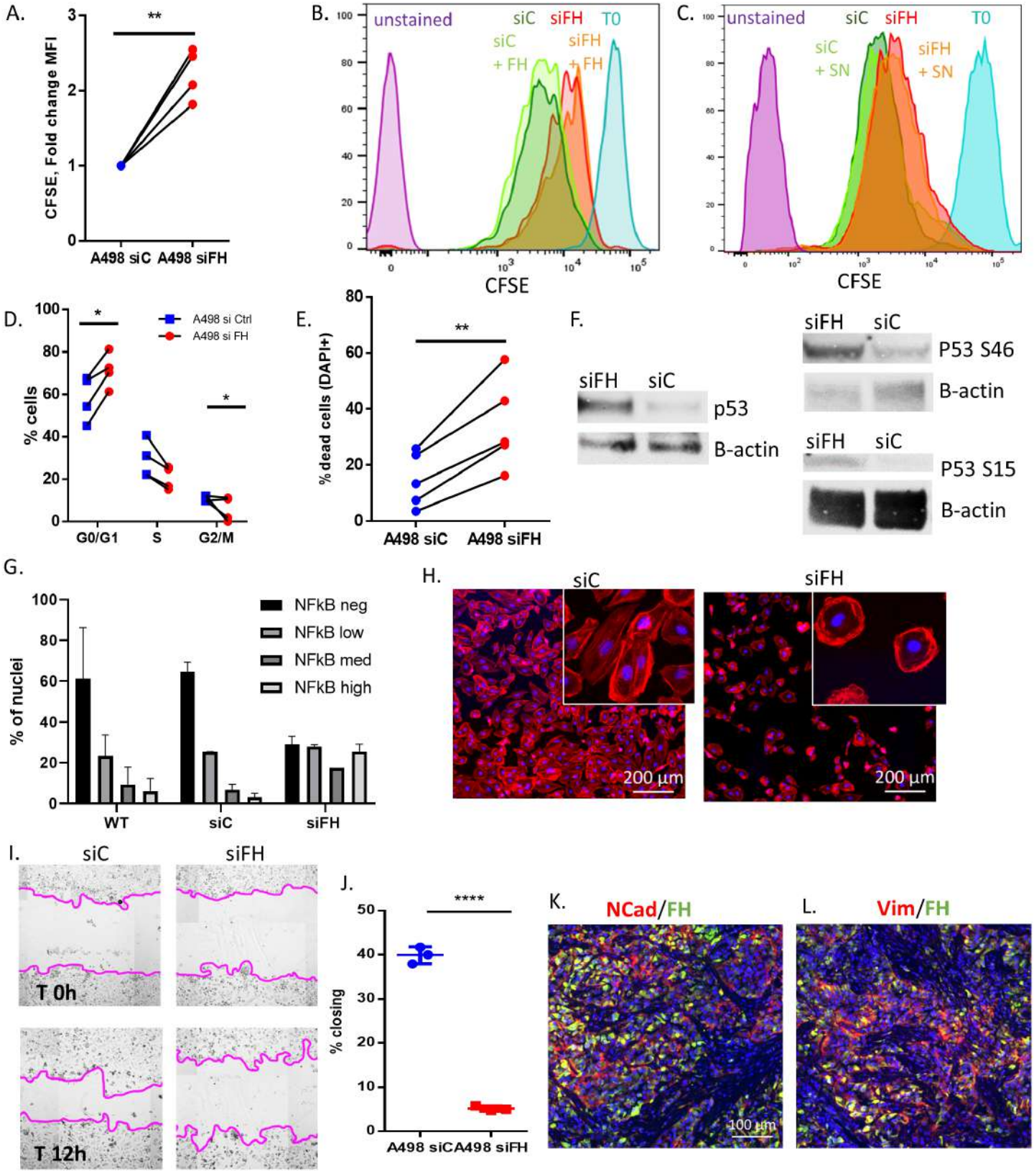

Figure 3: FH silencing modifies ccRCC tumor cell phenotype

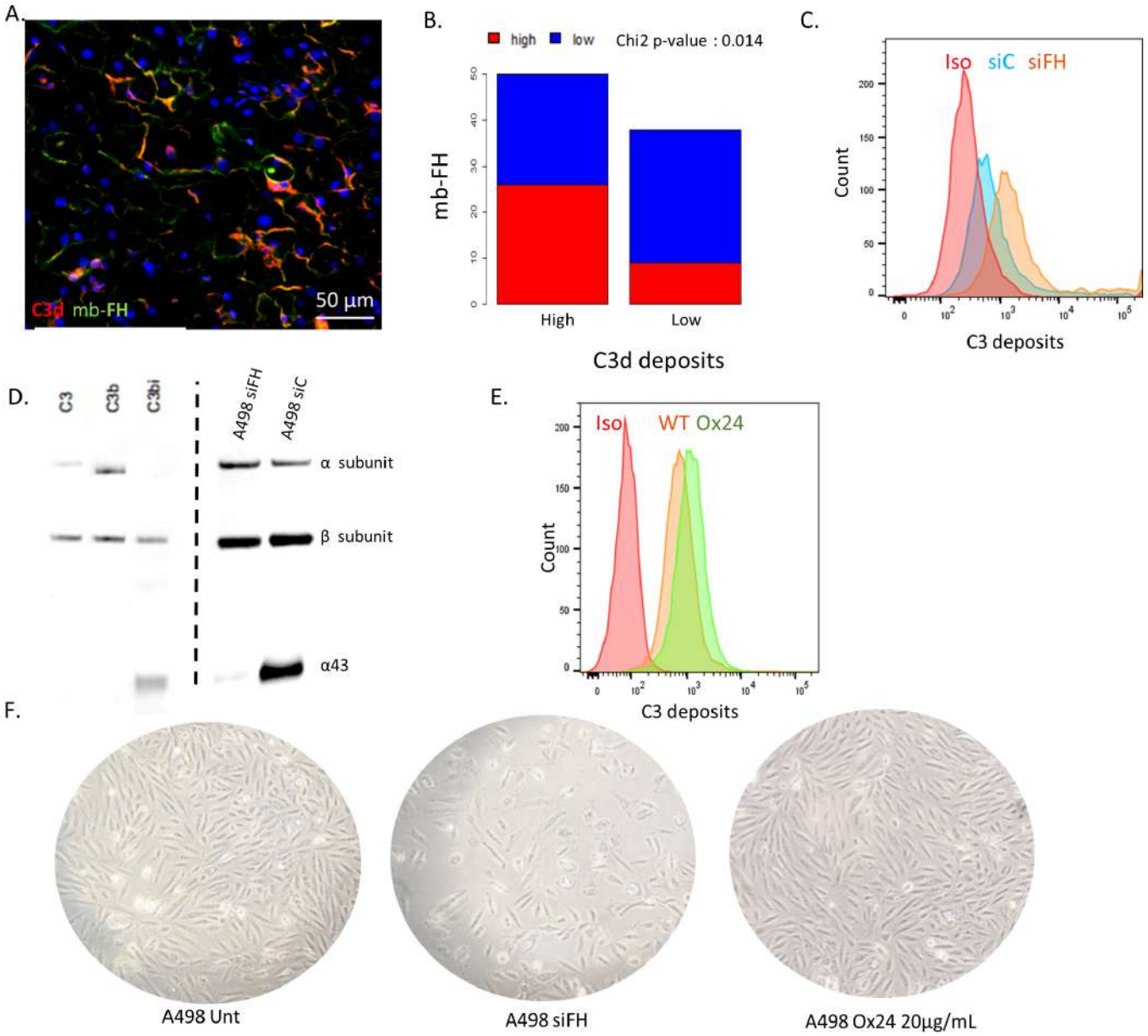

Figure 4: mb-FH regulates complement on tumor cells, but does not impact the cell phenotype.

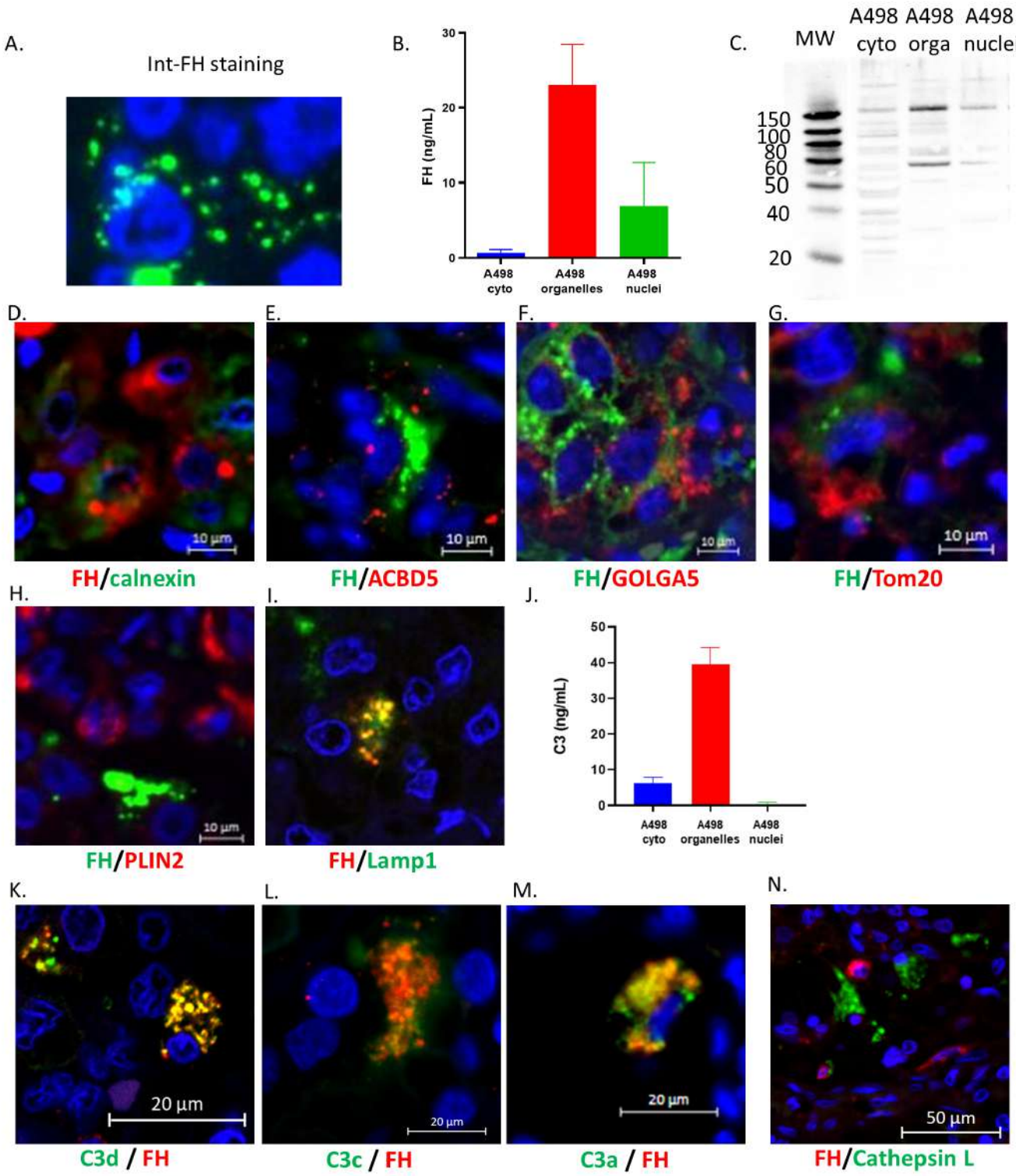

Figure 5: Int-FH is located in lysosomes and interacts with C3

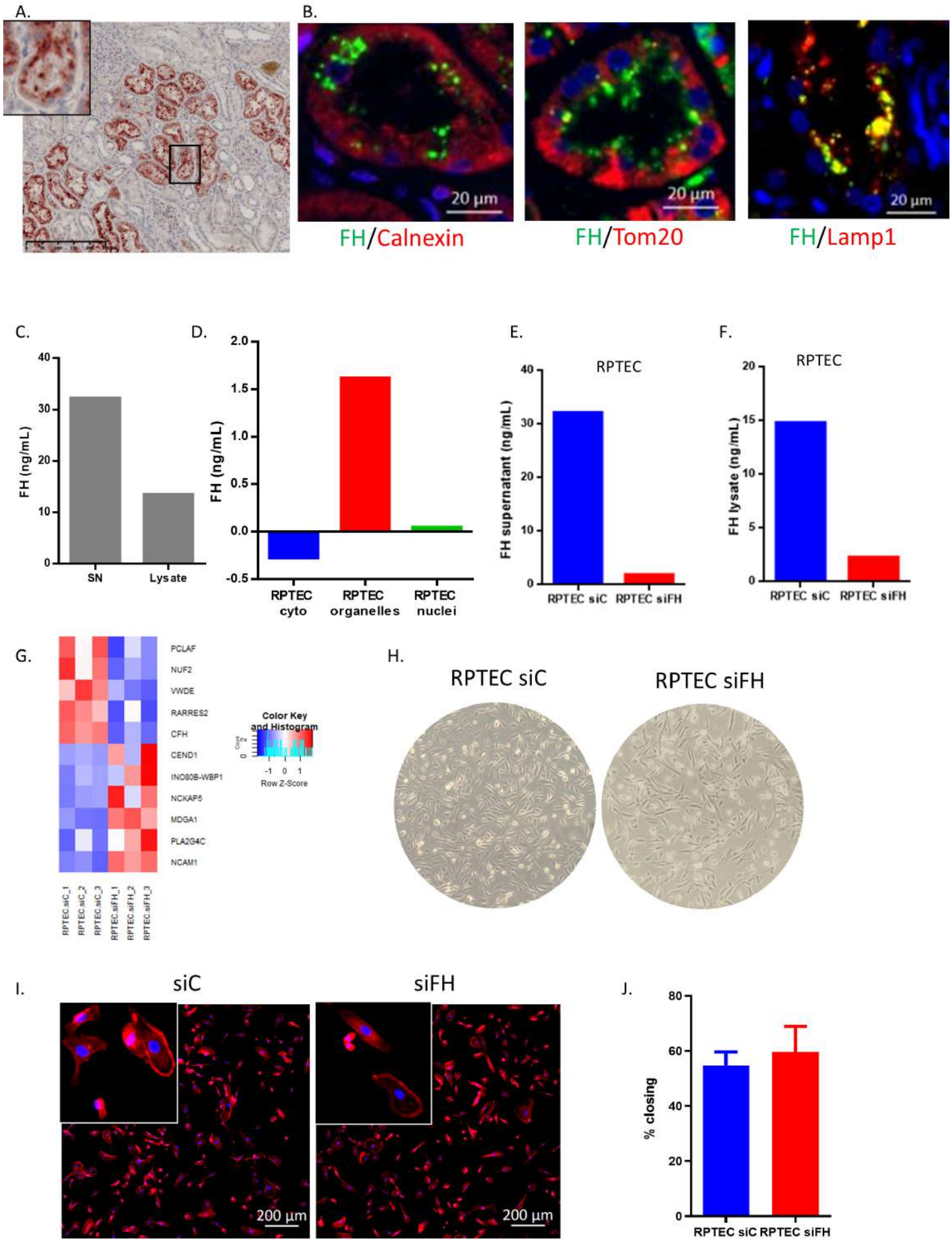

Figure 6: Silencing FH in RPTECs had no impact on the transcriptome and the phenotype

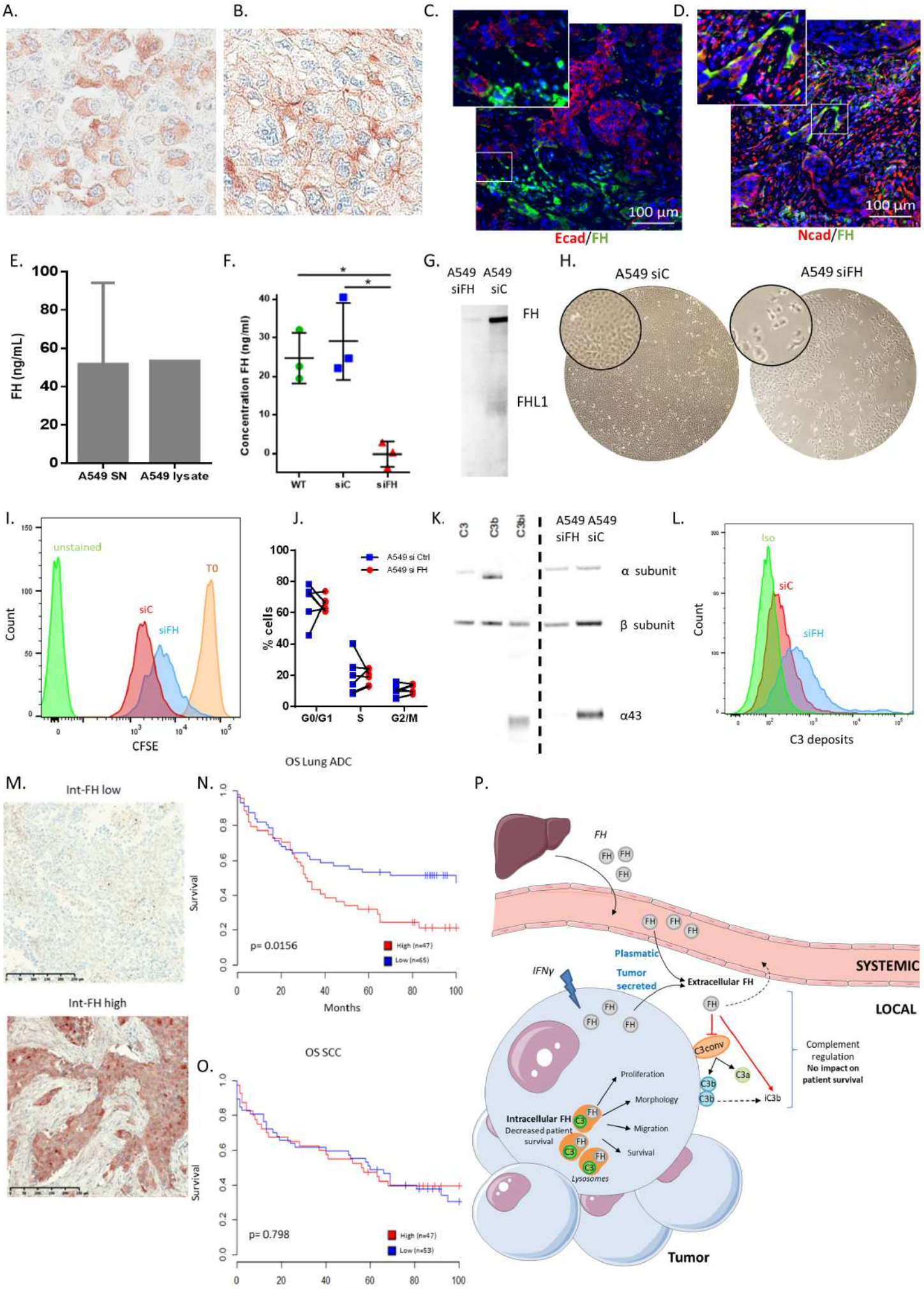

Figure 7. Int-FH but not mb-FH exerts a pro-tumoral effect on lung adenocarcinoma.

AACR American Association for Cancer Research

Cancer Immunology Research

Intracellular Factor H drives tumor progression independently of the complement cascade

Marie V Daugan, Margot Revel, Romane Thouenon, et al.

Cancer Immunol Res Published OnlineFirst May 26, 2021.